Deanship of Graduate Studies
Al – Quds University

Transporting nano particles across cell membranes

Prepared by:

Mohammed A. M. Abuawad

Supervisor: Dr. Khawla Qamhieh

M.Sc. Thesis

Jerusalem – Palestine

1436 / 2015

Deanship of Graduate Studies
Al – Quds University

Transporting nano particles across cell membranes

Prepared by:

Mohammed A. M. Abuawad

Supervisor: Dr. Khawla Qamhieh

A thesis submitted in partial fulfillment of requirement for the degree of Master of Science in Physics

Jerusalem – Palestine

1436/2015

Deanship of Graduate Studies
Al – Quds University

Thesis approval

Transporting nano particles across cell membranes

Prepared by: Mohammed A. M. Abuawad
Registration No: 21020266

Supervisor: Dr. Khawla Qamhieh

Master thesis submitted and accepted, date / / 2015

Names and signatures of the examining committee members are as follows:

1. Head of the committee: Dr. Khawla Qamhieh Signature: …….

3. Internal Examiner: Dr. Mohammad Abu Samreh Signature: .....

2. External Examiner: Dr. Wael Karain Signature: .....

Jerusalem – Palestine

1436/2015

Dedication

This thesis is dedicated to my mother, brothers, sisters and my deceased father. Besides, to all who suffer from genetic problems and cancer disease.

Declaration

I hereby declare that this thesis is based on the results found by myself. Materials of works found by other researchers are mentioned by references. This thesis, neither in whole nor in part, has been previously submitted for any degree. The work was done under the supervision of Dr. Khawla Qamhieh at Al–Quds University - Palestine.

Mohammed A. M. Abuawad

Acknowledgements

This thesis would not have been possible without the help, support and patience of my supervisor Dr. Khawla Qamhieh. I would like to thank her and many thanks to my teachers at Al-Quds University.

I am grateful to my friends without exception for their assistance. Thanks to my family and friends who stood beside me and encouraged me constantly.

Mohammed A. M. Abuawad

Abstract

We studied the forces affecting the nano particles penetration through another penetrable sphere like cell membrane by developing a free energy model. These nano particles could represent small ions, proteins and synthesized molecules like dendrimers. The reason behind studying penetration for these nano particles into cell membrane because of their potential to be used for drugs and cancer treatment in genes therapy.

We developed a free energy model based on the model that was produced by Dietrich (*Dietrich et al., 1997*) that handles the two interacting neutral particle spheres through penetration (no charges carried by spheres). By adding electrostatic interaction resulted from the charge of two interacting particles that may be owned by ions, molecules and proteins developed by Ohshima (*Ohshima, 2013*) to previous one we got a new free energy model. We concluded that the penetration of nanoparticles across other large particles increases dramatically when electrostatic interaction has been taken into account. Each parameter involved in electrostatic energy term has its special effect. We found through our research that penetration increases by increasing small nano particle charge while decreasing the salt concentration or the dielectric constant of medium contributes to increase the penetration.

Table of Contents

List of Tables

List of Figures

List of Abbreviations

ATP	Adenosine tri-phosphate
DNA	Deoxyribonucleic Acid
ICM-MS	Inductively Coupled Plasma Mass Spectroscopy
PAMAM	Polyamidoamine
PEs	Polyelectrolytes
RNA	Ribonucleic Acid
ssDNA	Single Stranded Deoxyribonucleic Acid
dsDNA	Double Stranded Deoxyribonucleic Acid
l_p	Persistence Length
HSA	Human Serum Albumin
DS	Dynamics Simulation
MDS	Molecular Dynamics Simulation
bp	base-pair
DLS	Dynamic Light Scattering
CTEM	Cryogenic Transmission Electron Microscopy
SSFS	Steady State Fluorescence Spectroscopy
SOPC	1-stearoyl-2-oleoyle-sn-glycero-3-phosphocholine
DMPC	1, 2-dimyristoyl-sn-glycero-3-phosphorylcholine

Chapter One

Introduction

1.1 Introduction

Gene therapy has been demonstrated to be a promising method in healing cancer and genetic diseases. Gene therapy derives its name from the idea that genetic materials can be used to supplement or alter gene expression within a specific cell population, thereby manipulating the cellular processes (*Mahato and Kim, 2002*). Hence, genetic materials could be targeted to tumor cells (*Lasic and Tcmpleton, 1997*). During their pass, it suffers from lots of barriers in the process of delivery like DNA degradation and decomplexation (*Patri et al., 2005*). Passing particles inward and outward the cell membrane is an application involving cell membrane interaction used to drag nano particles like ions and drugs into cell and vise versa. Some applications represented in viruses entering living cell through the process of endosomes. This process causes fusion of viral membrane with endosome membrane, also thus process involves adhesion and tension for membrane (*Deserno and Gelbart, 2002*). The large particle may be wrapped by lipid membrane while the small one tends to be penetrated. For example, dendrimer interacts through wrapping with lipid membrane as it approaches cellular membrane. This interaction is applied in gene therapy and chemotherapy to cancer cells. There are many methods for transferring nano particles into cytosol of cells which include disruption of endosomes, namely, sponge effect, direct micro injection of nano materials into cells (*Ayush and Francesco, 2009*), electro portion and conjugation of natural cell penetrating to nano materials (*Tkachenko et al., 2003*).

Alternative means of membrane translocation of nano scale sized material rely on intelligent surface structure design. Typically, nano material interactions with cell membranes are dedicated by chemical functionalities on the surface in addition to their

shape and size. For example, peptides cross cell membrane by adopting α–helical structure (*Bernardi, 2004*).

1.2 Cell membrane

The basic constituent building block in membrane cell is lipids. Lipids are used as fuel as a form of fat which used to store potential energy to be used as Adenosine tri-phosphate energy units (ATP). It provides internal organs protection through coating as well. Also fat is a bad heat conductor - the property that makes excellent insulator from medium. There are some compounds derived from lipids which are important building blocks of biologically active material for living substances in all animals, i.e., lipoproteins are a constituent of cell walls and they provide essential fatty acid. Figure 1.1 shows the basic structure of membrane.

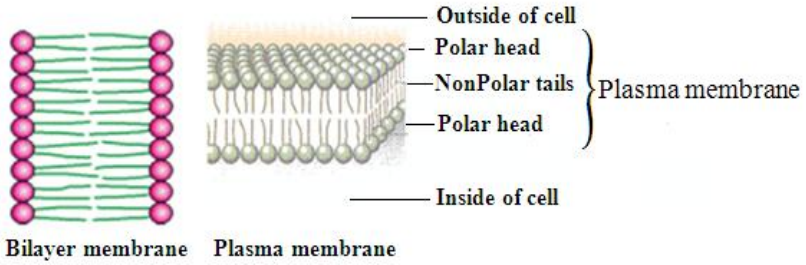

Figure 1.1: Membrane structure (*Gurr et al., 2002*)

The reason behind understanding the chemical structure of lipids and membrane is to enables us to analyze, to predict and to study the interaction between nano particles and cell membrane. It serves us in many applications relevant to medicine and drugs in human body. The solubility property depends mainly on hydrocarbon chain length and the number of bonds. The mentioned factors affect directly the physical properties like melting point. For example, double bond leads to disorder of chemical structure conferring it low melt point. The longer chain is more hydrophobic and less soluble. The number of carbon bonds (saturation) play important role in solubility. Hence,

double bond increases solubility as well as determines compound physical state (*Gurr et al., 2002*).

1.3 Transporting nano particles across cell membranes

Transporting nano particles inward and outward cell depends mainly on their size and nature. For example, ions like sodium and calcium ions (Na^{+}, Ca^{+2}) are so small (their radii are 0.095 *nm*, 0.099 *nm*, respectively). Membrane proteins of various kinds have been shown to act as transporters, their size ranges from 1 to 100 *nm* (*Lodish et al., 2000***;** *Deserno and Gelbart, 2002*). Figure 1.2 shows the protein A approaching cell membrane as a transporting vesicle to cell membrane.

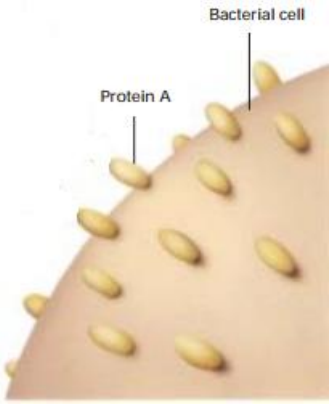

Figure 1.2: Experimental photo for a protein vesicle approaching bacterial cell surface membrane (*Lodish et al., 2000*)

Small and non-polar molecules like oxygen molecule (O_2), carbon dioxide molecule (CO_2) can diffuse across lipid bilayer through plasma permeable membrane (*Gurr et al., 2002*). Since many applications require breaching cell membrane barriers to reach cytosolic or nucleus of cell. There are many applications related to cell membrane like budding and subsequent vesiculation of lipid bilayer membranes essential for transport in biological cells. Buds formation due to membrane spontaneous curvature and viral budding (*Dasgupta et al., 2013*), designing efficient drug delivery systems and other

nano engineered techniques for medical diagnosis are biological examples of interaction with membrane (*Chithrani et al., 2006*). The uptake of small particles by cells such as elongated viruses have been found to form patterns on cell membrane (*Kubo et al., 2009*). For example, ellipsoidal nano particles are used for drugs delivery and as markers in cell biology (*Xu et al., 2011***;** *Chithrani et al., 2006*). Great efforts have been made to treat cancers, so lots of drugs which have been developed by pharmaceutical companies require from us to study their interaction with membrane. However, low solubility and poor biocompatibility have limited their clinical applications (*Jones and Zhang, 2008*).

1.4 Dendrimers as nano particles

Dendrimers are repetitively branched and symmetric molecules that often adopt spherical shape (Ö*rberg et al., 2007*). We will present their structure and interactions with biomolecules because of their potential in interaction.

1.4.1 Dendrimers structure

Dendrimers are a class of artificial macromolecules with a tree-like (hyper branched) structure, the interior layers from the core of the dendrimer to the surface groups have a homogeneous structure among the branching points. The branching units are described by generation, i.e., G_n such that G denotes to dendrimer characterized by generation number n, which is defined to be the number of branching points (*Ainalema and Nylander, 2011*). Dendrimer structure is shown as in Figure 1.3.

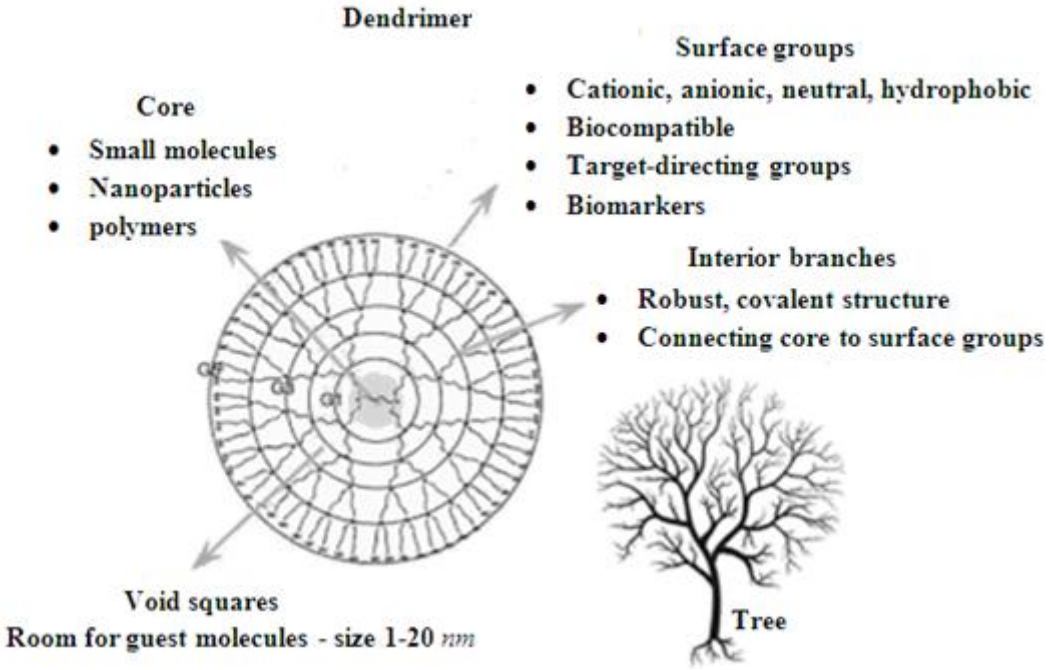

Figure 1.3: Dendrimer structure (*Ainalema and Nylander, 2011*)

Table 1.1 exhibits the dendrimer properties such molecular weight (*M*), charge (*Z*) which is carried by amine functional groups and the radius of dendrimer (*a*).

Table 1.1: Physical data for Polyamidoamine (PAMAM) dendrimers - ethylene mine core (*Ainalema and Nylander, 2011*)

Dendrimer G_n	Weight [M/g mol^{-1}]	Charge Z [e]	Radius a [nm]
1	1430	8	1.1
2	3256	16	1.45
3	6909	32	1.8
4	14215	64	2.25
5	28826	128	2.7
6	58048	256	3.35
7	116493	512	4.05
8	233383	1024	4.85
9	467162	2048	5.7
10	934720	4096	6.75

Surface charge density (σ) and volume charge density (ρ) can be calculated from the radius (*a*) and the charge (*Z*). For example, σ and ρ for dendrimer G_2 are equal to 0.60 e/nm^2, 1.25 e/nm^3, respectively. Various factors for dendrimer structure such as the generations, spacer lengths, environments various concentrations, valences of salt ions

and temperatures needed to be optimized for biomedical applications. Additionally, to overcome barriers in transporting process (*Mahato et al., 2002*). For example, the structure of G_2 dendrimer is shown as in Figure 1.4.

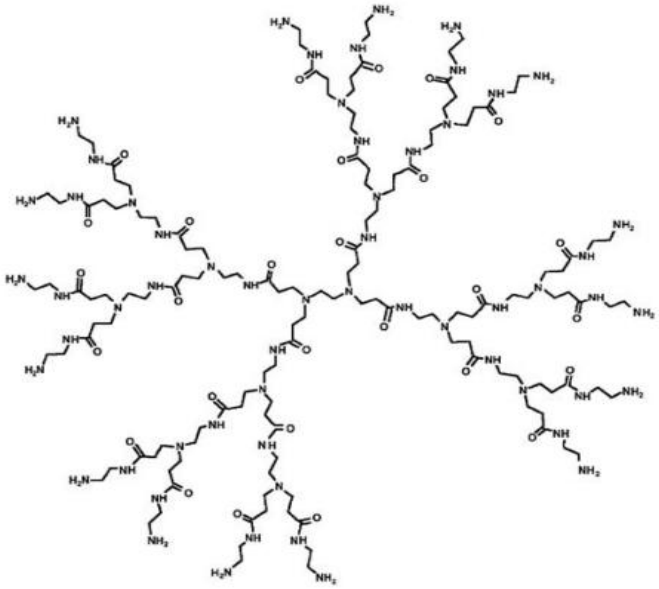

Figure 1.4: G_2 Polyamidoamine (PAMAM) dendrimer with ethylenedamine core and 16 amine functional groups-NH_2 (*Ainalema and Nylander, 2011*)

Researchers adopted mathematical models to solve the efficient shape and size of nanoparticles in the process of wrapping and penetration through interaction with cell membrane (*Ainalema and Nylander, 2011*; *Benoit and Saxena, 2007*). Acetylated G_5 dendrimer penetrates through cell membrane leaving a hole as shown in Figure 1.5.

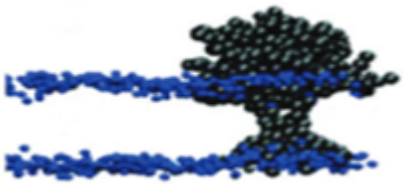

Figure 1.5: Nanoparticle acetylated G_5- Polyamidoamine (PAMAM) as a dendrimer can penetrate through cell membrane bilayer (*Lee and Larson, 2011*)

1.4.2 Interaction of dendrimers with molecules

Dendrimers interact with biomolecules as the following:

1. Interaction with small molecules like drugs or imaging molecules.

Dendrimers like Polyamidoamine (PAMAM) have a hydrophobic core and a hydrophilic surface layer. This characteristic offers the opportunity to dissolve poorly soluble. Non covalent or covalent attachments of drugs to dendrimers were reported to significantly affect the dissolution rate, the aqueous solubility, the stability and other physicochemical properties of the drugs in physiological conditions (*Duncan and Izzo, 2005*).

2. Interaction with linear polyelectrolytes (PEs) like Deoxyribonucleic Acid (DNA).

Gene materials and dendrimers may form complexes on the basis of electrostatic interactions that are convenient for delivery. For instance, the delivery of short interfering Ribonucleic Acid (RNA) into target cells using Polyamidoamine (PAMAM) dendrimers have been reported in experiments for studying gene functions as well for identifying and validating new drug targets (*Liu et al., 2012*). Linear gene material has various stiffness, i.e. DNA. DNA has a negative charge density of one charge per 0.17 *nm*. The experimental values of persistence length (l_p) for single stranded DNA (ssDNA) ranges from 0.75 to 3.0 *nm* while for double stranded DNA (dsDNA) is about 50 *nm* (*Watson and Crick, 1953*). For RNA, there is a large range of persistence length (l_p) (*Chen et al., 2012*).

3. Interaction with membranes.

Biomembranes play a central role in determining the structure and function of all biological cells. They serve as an interface between different organelles within a cell. Dendrimers may penetrate through the lipid bilayer membrane to carry out delivery. Experimental studies have shown that dendrimers can cause membrane disruption

through the formation of membrane holes and the expansion of preexisting defects (*Hong et al., 2004*). Moreover, the surface group of dendrimers may be modified with nano technology to attack the specific target of ill cells.

4. Interaction with proteins or peptides.

Dendrimers may interact with proteins, such as Human Serum Albumin (HAS), which is the most abundant protein in the blood. It has been found that dendrimers can bind with it through hydrophilic interactions. Further, proteins-peptides also play critical roles in the release of drugs in the interior of dendrimers (*Mahato et al., 2002*). Additionally, the dendrimers possibly come into a contact with specific protein targets such as membrane proteins and molecular motors. It has been shown that dendrimers encapsulate or interpenetrate a Polyelectrolyte (PE) chain depending on the salt concentration, size and charge density of the dendrimer and the Polyelectrolyte (PE) (*Welch and Muthukumar, 1998*). Bead spring simulations showed that the Polyelectrolyte (PE) is wrapped around the dendrimer surface, leading to decrease in the gyration radius of the dendrimer (*Lyulin et al., 2005*). But with longer chain that had more charges and more chain adsorbed into the dendrimer than were necessary for dendrimer neutralization then the role of electrostatic interaction appears. It has been shown that a strong electrostatic interaction of the divalent chain induced a decrease in the dendrimer size and an increase in the dehydration degree of the chain (*Lyulin et al., 2008*) while the size of the polyelectrolyte (PE) chain increases and the shape changes from oblate to prolate using Molecular Dynamic Simulation (MDS) technique (*Mahato and Kim, 2002*).

1.5 Compaction of DNA with cationic particles

Compacted DNA is achieved by wrapping the DNA 1.75 turns around positively charged histone proteins to form the so-called nucleosome core particles (*Kornberg, 1977*). DNA compaction is accompanied with a loss of conformational entropy which leads to increase the bending of the stiff double helix and increase intermolecular electrostatic repulsion (*Bloomfield, 1996*). It is important in gene therapy also it is suitable for living cell size to be contained and against degradation. Dynamic Light Scattering (DLS) was used to study the interaction between DNA and dendrimers as a function of the charge ratio - the ratio between the number of primary ammine groups on the dendrimer and the phosphate groups on DNA. The study showed that wrapping process is affected by that ratio. There are other factors that affect the interaction of nano particles with cell membrane represented in neutral surface charge on nano particle that minimize cellular interaction. Hence, functional groups on the nano particle and surface core primary determine many important nano material properties such as solubility, macro molecules and cell surface interaction. Using nano particles in wrapping and penetration process depends on the shape of colloidal, size, charge and salt concentration of the environment (*Ainalema and Nylander, 2011*). Figure 1.6 shows the main colloidal nano particle morphology.

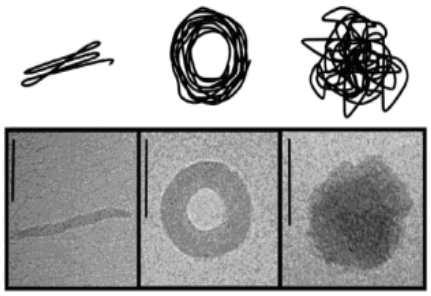

Figure 1.6: Colloidal morphology rods, toroids and globular (*Ainalema and Nylander, 2011*)

Wrapping nano particles such as viruses plays a key role in intercellular transport and soft matter systems. It was demonstrated that some particles are partially wrapped, some particles are fully wrapped and other particles remain unwrapped. Shape plays vital role in the process through dealing with drug delivery, gene therapy and other biological applications (*Dasgupta et al., 2013*). Dendrimer-DNA wrapping interaction is driven by electrostatic interaction which is affected by salt environment (*Maiti and Bagchi, 2006*). Figure 1.7 illustrates the interaction between different dendrimers and DNA under different pH environment

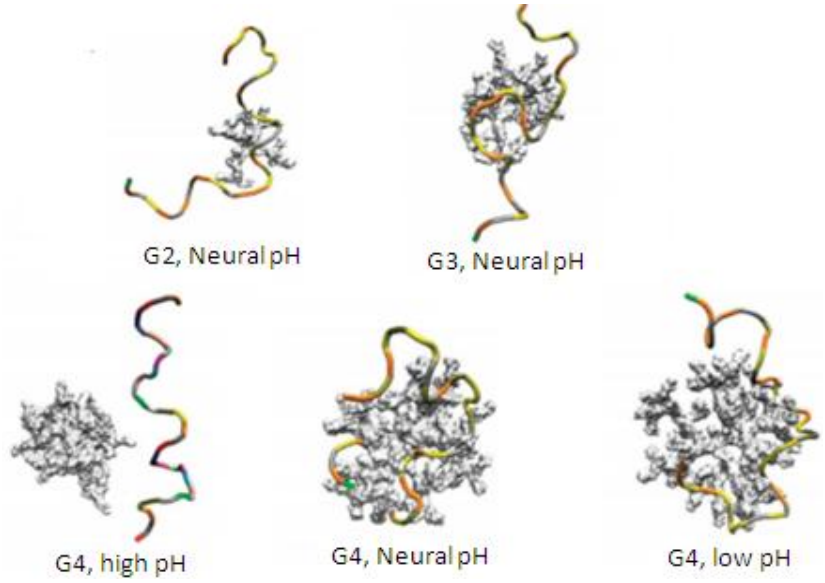

Figure 1.7: Different dendrimers interact with DNA at various pH environments (*Tian, and Ma, 2013*)

By modifying the study of interaction between polyelectrolyte(PE) chain and the dendrimer as a hard sphere that was done (*Schiessel, 2001*) by replacing the hard sphere with soft one (*Qamhieh and Khaleel, 2013*). They found that wrapping length is larger than the isoelectric length - the length of DNA needed to compensate the total charge of dendrimer. In their study they regarded dendrimer to be soft sphere – the radius is not constant through interaction with DNA as shown in Figure 1.8.

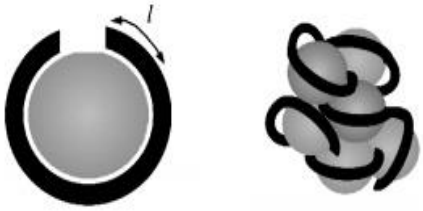

Figure 1.8: Wrapping DNA around dendrimer (*Qamhieh and Khaleel, 2013*)

Several factors that control the DNA/dendrimer complex relation such as the charge of the sphere, the linear charge density of the polymer, the ionic strength, the sphere radius, the flexibility of the polymer, number of dendrimer in the complex, pH number, type and the used generation of dendrimer.

Morphology of dendrimer-DNA aggregates was studied as a function of the dendrimer generation such as size, total charge and charge density, to provide further information of the condensation process. By using a mono disperse DNA sample of 4331 bp, dendrimers of generation G_1, G_2, G_4, G_6 and G_8. Three experimental techniques Cryogenic Transmission Electron Microscopy (CTEM), Dynamic Light Scattering (DLS) and Steady State Fluorescence Spectroscopy (SSFS) were used to show that the morphology of the aggregates transition from rods and toroids to globular aggregates with increasing dendrimer generation that affects surface charge density (*Ainalema and Nylander, 2011*).

Maiti and Bagchi performed 20 nanosecond long atomistic Molecular Dynamic (MD) simulations of G_2-G_4 dendrimer-ssDNA complexes in explicit water (*Maiti and Bagchi, 2006*). Their work showed that under some circumstances the degree of over compensation is very limited. During their work on dendrimer of G_4, they found that G_4 has enough positive charge 64 to neutralize the 37 charges on the ssDNA. They also noted that DNA first wrapped around dendrimer then after a period of time, it is penetrated inside the dendrimer which made dendrimer swollen (*Mahato and Kim,*

2002; *Maiti and Bagchi, 2006*; *Jonsson and Linse, 2001*). Figure 1.9 shows the complexes process between DNA and dendrimmer over the time period

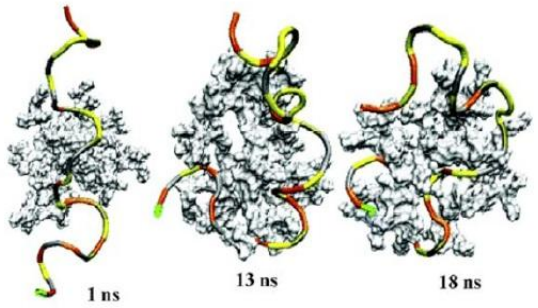

Figure 1.9: The formation of dendrimer-DNA complex over a period of time (*Maiti and Bagchi, 2006*)

Dietrich studied the penetration between two neutral penetrable spheres under the effect of adhesion and bending energies (*Dietrich et al., 1997*). They showed that penetration as a function of spheres sizes ratios, adhered area density and relative excess area Z_e (r, A, ε_{ab}) decreases either with increasing ratio(r) – the ratio between radius of small sphere to the radius of the large one - or decreasing relative excess area (ε_{ab}) or increasing adhered area density (A). They got the plot of penetration $Z_e(r)$ in two cases under elastic surface expansion modulus factor (K_a = 0.2 *N/m*) as shown in Figure 1.10.

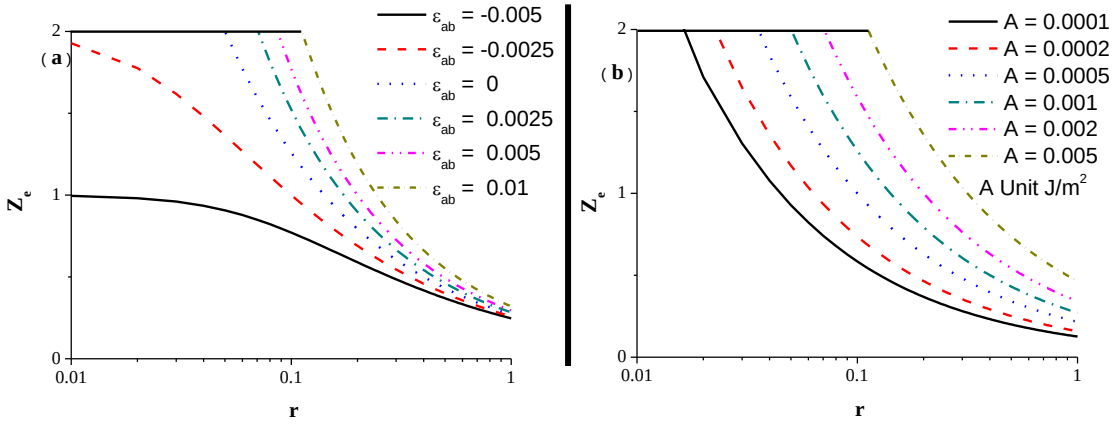

Figure 1.10: Penetration as a function of ratio Z_e (r) *in* two cases **a**) with constant adhered area density A = 0.001 *J/m*^{2} **b**) with constant relative excess area ε_{ab} = 0 (*Dietrich et al., 1997*)

1.6 Statement of the problem

The aim of our study is to understand the penetration of small nanoparticles such as ions, proteins and synthesized molecules into large particles like cell membrane. This study could play a vital role in gene therapy. Our efforts aim to generate a new model that contains adhesion, bending and electrostatic energy. Then investigating the impacts of the electrostatic energy on penetration when it is added to adhesion and bending energies. The reason behind concentrating on electrostatic energy beside adhesion and bending energies resides that synthesized molecules like dendrimers as interacting nanoparticles with cell membrane carry charges as pictured in Ohshima three-stage model(*Ohshima, 2010*). We used the three-stage model that supplies us with parameters that play important role in interpenetration process in addition to the parameters that was used in Dietrich model (*Dietrich et al., 1997*). Throughout this analytical study we are able to control the penetration process for cell membranes using charged particle rather than neutral ones to get the most desired transfection efficiency in gene therapy that could be applied in nano medicine and drugs delivery system into human cell membranes. This control could be achieved by controlling electrostatic parameters contained in electrostatic interaction.

Chapter Two

Theoretical Background

2.1 Introduction

We will develop a new free energy model based on Dietrich model (*Dietrich et al., 1997*) that was used for processing the penetration resulted from adhesion and bending energies. This new free energy model could be achieved by inserting the electrostatic energy that was proposed by Ohshima three-stage model (*Ohshima, 2013*) to the adhesion and bending energies (*Dietrich et al., 1997*). The two spheres were pictured as soft porous spheres involve interpenetration between each other. Therefore, the new free energy model is a perfect biophysical model explaining nano particles transport through cell membrane. The picture of electrostatic interaction between two spheres is illustrated in three stages as in Figure 2.1.

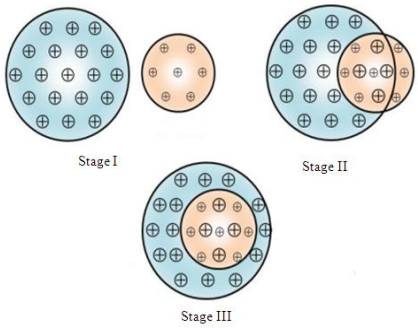

Figure 2.1: Electrostatic interaction between two charge porous sphere in three stages (*Ohshima, 2010*; *Ohshima, 2013*)

2.2 Interpenetration by electrostatic energy only

The electrostatic interaction between two porous charged spheres involves three stages according to Ohshima three-stage model as referred in Figure 2.1. Stage I is called before contact represented with region I. Stage II is called interpenetration stage represented with region II. Stage III is called engulfing stage represented with region III, we just used the second stage of interaction that involves interpenetration of two

spheres. The second stage is represented in region II (*Ohshima, 2013***;** *See Appendix B*).

Region I:

Region I is used at a separation distance *x* such that *x* ranges over the interval$[R + a, \infty]$. Stage I is used to bring the two nano particles for interaction. The electrostatic energy (E_{Stage1}) in stage I (before contact) involved in Region I is described as follows (*Ohshima, 2013*)

$$E_{Stage1}(x) = \frac{4\pi Ra\rho_1\rho_2}{\varepsilon_r\varepsilon_0\kappa^4}\left(\cosh(\kappa R) - \frac{\sinh(\kappa R)}{\kappa R}\right)\left(\cosh(\kappa a) - \frac{\sinh(\kappa a)}{\kappa a}\right)\frac{e^{-\kappa x}}{x} \tag{2.1}$$

The electrostatic force (F_{Stage1}) in Region I can be expressed as follows

$$F_{Stage1} = -\frac{dE_{Stage1}}{dx} \tag{2.2}$$

$$F_{Stage1} = \frac{4\pi Ra\rho_1\rho_2}{\varepsilon_r\varepsilon_0\kappa^4}\left(\cosh(\kappa R) - \frac{\sinh(\kappa R)}{\kappa R}\right)\left(\cosh(\kappa a) - \frac{\sinh(\kappa a)}{\kappa a}\right)\frac{(\kappa x + 1)e^{-\kappa x}}{x^2} \tag{2.3}$$

Region II:

Region II is used at a separation distance *x* where *x* ranges over the interval$[R - a, R + a]$. Stage II involves the interpenetration process for two nano particles. This stage will serve our modified free energy model. The electrostatic energy in stage II (E_{Stage2}) through interpenetration process is expressed as follows (*Ohshima, 2013*)

$$\begin{aligned} E_{Stage2}(x) = \frac{2\pi Ra\rho_1\rho_2}{\varepsilon_r\varepsilon_0\kappa^4 x}\Bigg[&\frac{1}{\kappa^2 Ra}\left\{1 + \frac{\kappa^2}{2}(x^2 - R^2 - a^2)\right\} \\ &+ \frac{\kappa^2}{24Ra}\ (x - R - a)^2\{x^2 + 2(R+a)x - 3(R-a)^2\} \\ &+ \left(1 - \frac{1}{\kappa^2 Ra}\right)e^{-\kappa x}\cosh(\kappa(R-a)) - \left(\frac{1}{\kappa R} - \frac{1}{\kappa a}\right)e^{-\kappa x}\sinh(\kappa(R-a)) \\ &- \left(1 + \frac{1}{\kappa R}\right)\left(1 + \frac{1}{\kappa a}\right)e^{-\kappa(R+a)}\sinh(\kappa x)\Bigg] \end{aligned}$$

(2.4)

The electrostatic force (F_{Stage2}) in Region II can be expressed as follows

$$F_{Stage2} = -\frac{dE_{Stage2}}{dx} \tag{2.5}$$

$$\begin{aligned} F_{Stage2}(x) = \frac{\pi R a \rho_1 \rho_2}{\varepsilon_r \varepsilon_0 \kappa^4 x^2}\Bigg[& \left(1+\frac{1}{\kappa R}\right)\left(1+\frac{1}{\kappa a}\right)\{(\kappa x+1)e^{-\kappa(x+R+a)} \\ & + (\kappa x-1)e^{\kappa(x-R-a)}\} + \left(1+\frac{1}{\kappa R}\right)\left(1-\frac{1}{\kappa a}\right)(\kappa x+1)e^{-\kappa(x+R-a)} \\ & + \left(1-\frac{1}{\kappa R}\right)\left(1+\frac{1}{\kappa a}\right)(\kappa x+1)e^{-\kappa(x-R+a)} \\ & + \kappa^2 R a\left\{1-\frac{1}{(\kappa R)^2}\right\}\left\{1-\frac{1}{(\kappa a)^2}\right\} - \frac{1}{\kappa^2 R a}\{(\kappa x)^2-1\} \\ & - \frac{\kappa^2}{4Ra}(x^2 - R^2 - a^2)^2\Bigg] \end{aligned} \tag{2.6}$$

Region III:

Region III is used at a separation distance *x* where *x* ranges over the interval$[0, R-a]$. Stage III involves the end of interpenetration process for two nano particles reaching the engulfing sate. The electrostatic energy (E_{Stage3}) in stage III is written as follows (*Ohshima, 2013*)

$$E_{Stage3}(x) = \frac{4\pi R a \rho_1 \rho_2}{\varepsilon_r \varepsilon_0 \kappa^4 x}\left[\frac{(\kappa a)^2 x}{3R} - \left(1+\frac{1}{\kappa R}\right)e^{-\kappa R}\left(\cosh(\kappa a) - \frac{\sinh(\kappa a)}{\kappa a}\right)\sinh(\kappa x)\right] \tag{2.7}$$

The electrostatic force (F_{Stage3}) in Region III can be expressed as follows

$$F_{Stage3} = -\frac{dE_{Stage3}}{dx} \tag{2.8}$$

$$F_{Stage3}(x) = \frac{4\pi R a \rho_1 \rho_2}{\varepsilon_r \varepsilon_0 \kappa^4 x^2}\left[\left((\kappa x)\cosh(\kappa x) - \sinh(\kappa x)\right)\left(1+\frac{1}{\kappa R}\right)e^{-\kappa R}\left(\cosh(\kappa a) - \frac{\sinh(\kappa a)}{\kappa a}\right)\right] \tag{2.9}$$

Where *a*, *R* are the radii of two charged porous spheres carrying the volume charge densities ρ_1, ρ_2, respectively. ε_r is dielectric constant of the spheres, ε_0 is permittivity of free space (vacuum permittivity), x is the separation distance between two interacting spheres centers and κ Deybe-Huckel parameter (Debye screening length) which is defined according to (*Ohshima, 2010*):

$$\kappa = \left(\frac{1}{\varepsilon_r \varepsilon_0 K_B T} \sum_{i=1}^{N} z_i^2 e^2 n_i \right)^{\frac{1}{2}} \tag{2.10}$$

K_B is Boltzmann constant, T is the temperature, z_i is a valence of ionic species in electrolyte and n_i is the bulk concentration of ionic species (density number).

For obtaining the penetration as function of ratio $Z_e(r)$ where the ratio r is (a/R), we get it by differentiating electrostatic energy of the second stage (E_{Stage2}) as follows

$$\frac{dE_{Stage2}}{dz} = \frac{dE_{Stage2}}{dx} \frac{dx}{dz} \tag{2.11}$$

Where the separation distance $x = R + a - az$. So substituting $dx/dz = -a$ into Eq. (2.11) as follows

$$\frac{dE_{Stage2}}{dz} = \frac{dE_{Stage2}}{dx} (-a) \tag{2.12}$$

Multiplying Eq. (2.6) with a negative sign and then substituting it in Eq. (2.12) as follows

$$\begin{aligned} \frac{dE_{Stage2}}{dz} = \Bigg(\frac{\pi R a \rho_1 \rho_2}{\varepsilon_r \varepsilon_0 \kappa^4 x^2} \Bigg[& \left(1 + \frac{1}{\kappa R}\right)\left(1 + \frac{1}{\kappa a}\right)\{(\kappa x + 1)e^{-\kappa(x+R+a)} + (\kappa x - 1)e^{\kappa(x-R-a)}\} \\ & + \left(1 + \frac{1}{\kappa R}\right)\left(1 - \frac{1}{\kappa a}\right)(\kappa x + 1)e^{-\kappa(x+R-a)} + \left(1 - \frac{1}{\kappa R}\right)\left(1 + \frac{1}{\kappa a}\right)(\kappa x + 1)e^{-\kappa(x-R+a)} \\ & + \kappa^2 R a \left\{1 - \frac{1}{(\kappa R)^2}\right\}\left\{1 - \frac{1}{(\kappa a)^2}\right\} - \frac{1}{\kappa^2 R a}\{(\kappa x)^2 - 1\} \\ & - \frac{\kappa^2}{4Ra}(x^2 - R^2 - a^2)^2 \Bigg] \Bigg) a \end{aligned} \tag{2.13}$$

Eq. (2.13) can be solved numerically to get penetration values $Z_e(r)$.

2.3 Analytical model for the interpenetration under total energy

The total energy (E_T) is defined to be the sum of adhesion energy (E_a), the bending energy (E_b) and the electrostatic energy in the second stage (E_{Stage2}) as follows

$$E_T = E_a + E_b \pm E_{Stage2}$$

$$E_T = E_a + E_b + \begin{cases} +E_{Stage2}\text{ , repulsion interaction} \\ -E_{Stage2}\text{ , attraction interaction} \end{cases} \quad (2.14)$$

So the picture of two penetrable spheres before interaction is illustrated as shown in Figure 2.2.

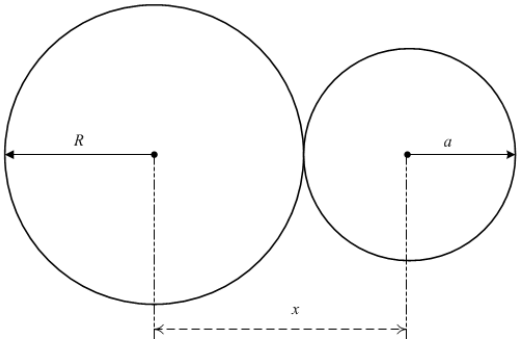

Figure 2.2: The two spheres before interaction

While the illustrated system through interpenetration when the sphere of small radius a starts to penetrate the large one whose radius *R* is shown as in Figure 2.3.

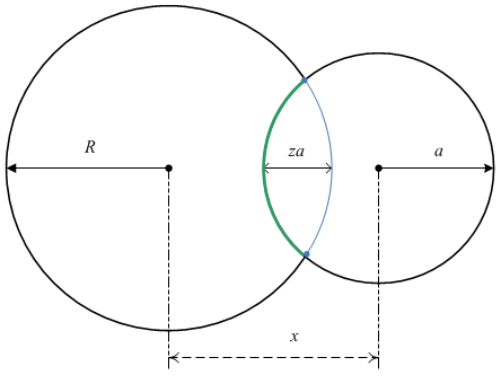

Figure 2.3: The two spheres through interpenetration

The parameters involved in the process of the interaction that determine the distance between spheres centers in stage II are the radii of two spheres *a, R* and the penetration

value(z). For $a < R$, the separation distance between two spheres centers(x), x can be defined as

$$x = R + a - az \quad (2.15)$$

The value z defined intern of contact angle (θ) as shown in Figure 2.4.

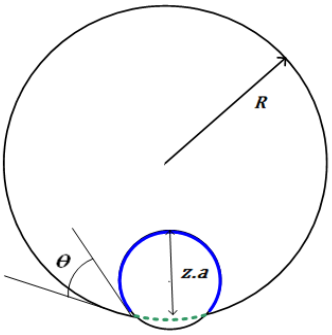

Figure 2.4: Contact angle ɵ (*Dietrich et al., 1997*)

The value (z) is given by the relation as in Dietrich model (*Dietrich et al., 1997*)

$$z = 1 + \cos \theta \quad (2.16)$$

Mathematically, $\cos \theta$ function resides on the interval [-1, 1]. Hence, penetration value z after substituting the start and the end of interval in Eq. (2.16) ranges over the interval $[0, 2]$. Physically, the dimensionless quantity (z) represents how many radius of small sphere penetrates into large one. Now representing the free energy (E_{ab}) as the sum of adhesion energy (E_a) and bending energy (E_b) as follows (*Dietrich et al., 1997*)

$$E_{ab} = E_a + E_b \quad (2.17)$$

Each one can be defined by the following relation (*Dietrich et al., 1997*)

$$E_a = -AS_a \quad (2.18)$$

Such that A is substrate adhesion energy density and S_a is referred as the adhered area from small sphere to large one which is defined by the relation (*Dietrich et al., 1997*)

$$S_a = 2\pi a^2 z \quad (2.19)$$

The negative sign in adhesion energy indicates that the adhesion energy generates attraction force. The bending energy simplified with (*Dietrich et al., 1997*)

$$E_b = \frac{1}{2} k_a \frac{(S - S_0)^2}{S_0} \qquad (2.20)$$

Where k_a is the elastic surface expansion modulus factor, S_0 is surface area at rest (zero tension) such that $S = \pi a^2 z^2$ and $S_0 = 4\pi R^2 \varepsilon_{ab}$, ε_{ab} refers to relative excess in surface area, Eq. (2.17) can be rewritten as

$$E_{ab} = -AS_a + \frac{1}{2} k_a \frac{(S - S_0)^2}{S_0} \qquad (2.21)$$

Substituting Eq. (2.19) and the values of *S*, S_0 into Eq. (2.21), we got

$$E_{ab} = -2\pi \mathrm{A} a^2 z + \frac{1}{2} k_a \frac{(\pi a^2 z^2 - 4\pi R^2 \varepsilon_{ab})^2}{4\pi R^2 \varepsilon_{ab}} \qquad (2.22)$$

Simplifying Eq. (2.22), we got

$$E_{ab} = -2\pi \mathrm{A} a^2 z + \frac{1}{2} k_a \frac{(\pi^2 a^4 z^4 + 16\pi^2 R^4 {\varepsilon_{ab}}^2 - 8\pi^2 a^2 R^2 \varepsilon_{ab} z^2)}{4\pi R^2 \varepsilon_{ab}} \qquad (2.23)$$

Eq. (2.23) represents the free energy of the system under the effect of adhesion energy (E_a) and bending energy (E_b).

Differentiating the free energy E_{ab} (z), to get the penetration at equilibrium $Z_e(r)$

$$\frac{dE_{ab}}{dz} = -2\pi A a^2 + \frac{1}{2} k_a \frac{(4\pi^2 a^4 z^3 - 16\pi^2 a^2 R^2 \varepsilon_{ab} z)}{4\pi R^2 \varepsilon_{ab}} \qquad (2.24)$$

Eq. (2.23) was used to calculate the free energy $E_{ab}(x)$ as follows

$$E_{ab} = -2\pi \mathrm{A} a(R + a - x) + \frac{1}{2} k_a \frac{(\pi^2 (R + a - x)^4 + 16\pi^2 R^4 {\varepsilon_{ab}}^2 - 8\pi^2 R^2 \varepsilon_{ab} (R + a - x)^2)}{4\pi R^2 \varepsilon_{ab}} \qquad (2.25)$$

And the free force $F_{ab}(x)$ can be obtained as the follows

$$F_{ab} = -\frac{dE_{ab}}{dx} = -\frac{dE_{ab}}{dz} . \frac{dz}{dx} \qquad (2.26)$$

By using Eq. (2.24) and Eq. (2.15), then Eq. (2.26) can be rewritten as

$$F_{ab} = \left(-2\pi A a + \frac{1}{2} k_a \frac{(4\pi^2 a^3 z^3 - 16\pi^2 a R^2 \varepsilon_{ab} z)}{4\pi R^2 \varepsilon_{ab}} \right) \qquad (2.27)$$

For obtaining the total free energy of the system (E_T), we can sum the adhesion and bending energies (E_{ab}) as in Eq. (2.25) into electrostatic energy of the second stage (E_{Stage2}) as in Eq. (2.4) as follows

$$E_T = -2\pi \mathrm{A} a(R + a - x) + \frac{1}{2}k_a \frac{(\pi^2(R + a - x)^4 + 16\pi^2 R^4 {\varepsilon_{ab}}^2 - 8\pi^2 R^2 \varepsilon_{ab}(R + a - x)^2)}{4\pi R^2 \varepsilon_{ab}} + \left(\frac{2\pi R a \rho_1 \rho_2}{\varepsilon_r \varepsilon_0 \kappa^4 x}\left[\frac{1}{\kappa^2 R a}\left\{1 + \frac{\kappa^2}{2}(x^2 - R^2 - a^2)\right\}\right.\right. + \frac{\kappa^2}{24Ra}\ (x - R - a)^2\{x^2 + 2(R + a)x - 3(R - a)^2\} + \left(1 - \frac{1}{\kappa^2 R a}\right)e^{-\kappa x}\cosh(\kappa(R - a)) - \left(\frac{1}{\kappa R} - \frac{1}{\kappa a}\right)e^{-\kappa x}\sinh(\kappa(R - a)) \left.\left. - \left(1 + \frac{1}{\kappa R}\right)\left(1 + \frac{1}{\kappa a}\right)e^{-\kappa(R+a)}\sinh(\kappa x)\right]\right) \quad (2.28)$$

Eq. (2.28) can be solved numerically by finding the extreme values for studying penetration function of ratio $Z_e(r)$ in equilibrium.

The total free force of the system (F_T) can be obtained as follows

$$F_T = -\frac{dE_T}{dx} \quad (2.29)$$

$$F_T = -2\pi \mathrm{A}a - \frac{1}{2}k_a \frac{\left(\pi(R+a-x)^3 - 4\pi R^2 \varepsilon_{ab}(R+a-x)\right)}{R^2 \varepsilon_{ab}}$$

$$+ \left(\frac{\pi R a \rho_1 \rho_2}{\varepsilon_r \varepsilon_0 \kappa^4 x^2}\left[\left(1+\frac{1}{\kappa R}\right)\left(1+\frac{1}{\kappa a}\right)\{(\kappa x+1)e^{-\kappa(x+R+a)}\right.\right.$$

$$+ (\kappa x-1)e^{\kappa(x-R-a)}\} + \left(1+\frac{1}{\kappa R}\right)\left(1-\frac{1}{\kappa a}\right)(\kappa x+1)e^{-\kappa(x+R-a)}$$

$$+ \left(1-\frac{1}{\kappa R}\right)\left(1+\frac{1}{\kappa a}\right)(\kappa x+1)e^{-\kappa(x-R+a)}$$

$$+ \kappa^2 R a\left\{1-\frac{1}{(\kappa R)^2}\right\}\left\{1-\frac{1}{(\kappa a)^2}\right\} - \frac{1}{\kappa^2 R a}\{(\kappa x)^2-1\}$$

$$\left.\left. - \frac{\kappa^2}{4Ra}(x^2 - R^2 - a^2)^2\right]\right) \qquad (2.30)$$

Differentiating the total free energy (E_T) for obtaining extreme values using Eq. (2.13), Eq. (2.15) and Eq. (2.24) as follows

$$\frac{dE_T}{dz} = \frac{dE_{ab}}{dz} + \frac{dE_{Stage2}}{dz} = \frac{dE_{ab}}{dz} + \frac{dE_{Stage2}}{dx}.\frac{dx}{dz} \qquad (2.31)$$

$$\frac{dE_T}{dz} = k_a\left(\left(\frac{a}{2R}\right)^2 z^3 - \varepsilon_{ab} z\right) - A$$

$$+ a\frac{\pi R a \rho_1 \rho_2}{\varepsilon_r \varepsilon_0 \kappa^4 x^2}\left[\left(1+\frac{1}{\kappa R}\right)\left(1+\frac{1}{\kappa a}\right)\{(\kappa x+1)e^{-\kappa(x+R+a)}\right.$$

$$+ (\kappa x-1)e^{\kappa(x-R-a)}\} + \left(1+\frac{1}{\kappa R}\right)\left(1-\frac{1}{\kappa a}\right)(\kappa x+1)e^{-\kappa(x+R-a)}$$

$$+ \left(1-\frac{1}{\kappa R}\right)\left(1+\frac{1}{\kappa a}\right)(\kappa x+1)e^{-\kappa(x-R+a)} + \kappa^2 R a\left\{1-\frac{1}{(\kappa R)^2}\right\}\left\{1-\frac{1}{(\kappa a)^2}\right\}$$

$$- \frac{1}{\kappa^2 R a}\{(\kappa x)^2-1\}$$

$$\left. - \frac{\kappa^2}{4Ra}(x^2 - R^2 - a^2)^2\right] \qquad (2.32)$$

We can solve Eq. (2.32) numerically to study the electrostatic energy parameters in coincide with the adhesion and the bending energies' parameters together. For *z* values, we get its values under the effect of the adhesion, the bending and the electrostatic energies.

Chapter Three

Results and Discussions

3.1 Introduction

The present calculations have been done by essential tools for mathematical and modeling Maple software. Also we used Origin software by supplying it with data obtained from numerical analysis to get the plots. We obtained the penetration values of nanoparticles through larger particles under the effect of the total free energy represented with adhesion energy, bending energy and electrostatic energy in stage II through solving Eq. (2.32) numerically for studying penetration function $Z_e(r, A, \varepsilon_{ab}, \rho_1, \kappa, \varepsilon_r)$. We obtained Eq. (2.32) through the differentiation of the Eq. (2.28) that represents the total free energy of the system. Getting the effect of each parameter enable us to control the penetration process, this control could be applied in interpenetration process in the field of nano medicine and drugs delivery.

3.2 Electrostatic interaction between two penetrable spheres

In this section, we will show the three interaction regions between two penetrable porous spheres by applying three stage model developed by Ohshima (*Ohshima, 2013*). This model describes the three regions of electrostatic interaction between two nano particles spheres. We can assume that the small sphere has a radius *a*, the large one has a radius *R* and also both two penetrable spheres carry two volume charge densities differ in kind ρ_1, ρ_2, respectively. By choosing $a = 8\ nm$ to be the radius for a small porous nano particle soft sphere carrying volume charge density $\rho_1 = -5\ e/nm^3$ and the large one have a radius of $R = 10\ nm$ carrying volume charge density $\rho_2 = 0.5\ e/nm^3$. Both two spheres immersed in a 1:1 solution that corresponds to a 1:1 solution giving a salt concentration 10 mM with dielectric constant $\varepsilon_r = 78$. After that, Ohshima model was applied to plot the electrostatic interaction in the three regions where Eq. (2.1), Eq.

(2.3) for region I, Eq. (2.4), Eq. (2.6) for region II and Eq. (2.7), Eq. (2.9) for region III. The obtained results were plotted in Figure 3.1.

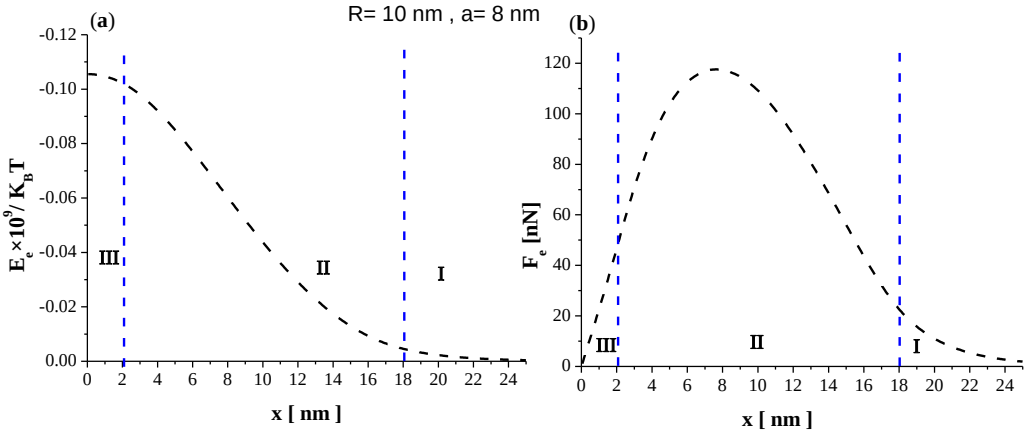

Figure 3.1: **a**) Electrostatic energy $E_e(K_BT)$ **b**) Electrostatic force $F_e(n\text{N})$ between two spheres centers of radii a = 8 *nm*, R = 10 *nm* carrying ρ_1 = -5 e/nm^3, ρ_2 = 0.5 e/nm^3 volume charge densities, respectively. Dielectric constant ε_r = 78 and Debye screening length κ = 0.3 nm^{-1} (10 mM 1:1 solution) in three regions in both two cases.

As it can be seen in Figure 3.1, the electrostatic interaction is located in three regions: region I of electrostatic interaction scanned by the interval $[R + a, \infty]$ = [18 *nm*, ∞ *nm*] (both two spheres are not in touch), this stage does not serve us since the two spheres are not in a contact. Second region II of electrostatic interaction which describes the interpenetration stage process between two spheres located in the interval $[R- a, R + a]$ = [2 *nm*, 18 *nm*], at that stage, we will concentrate our work. Third region III of electrostatic interaction ranges over the interval $[0, R - a]$ = [0 *nm*, 2 *nm*] which describes the engulfing stage (small sphere engulfed by large one), the third stage represents the final stage of interaction that comes directly after the end of interpenetration. By concentrating on the second stage II that involves interpenetration process, we have seen maximum electrostatic interaction taking place in region II, especially in the first two third of second stage (*Ohshima, 2013*). The result we obtained is consistence with that obtained through studying the interaction between soft cylindrical porous nano particles (*Ohshima, 2010*). Our study differs by assuming

the two interacting particles to be spheres for continuing the model we propose and replacing the neutral particles (*Dietrich et al., 1997*) with charged ones as proposed by Ohshima (*Ohshima, 2013*). Mainly, electrostatic force appears from the charges of spheres (*Tomalia, 2010***;** *Ding et al., 2012***;** *Maiti and Bagchi, 2006*).

3.3 Effect of electrostatic energy parameters

In details, this section aims to discuss the impacts of the electrostatic interaction parameters, namely, volume charge density of interacting spheres ρ_1, ρ_2 and dielectric constant ε_r of interacting spheres as well the environment. Spheres sizes were expressed by their radii *a*, *R*, salt concentration of solution represented intern of Debye screening length κ^{-1}. We will discuss each parameter and its effect on electrostatic interaction in order to control penetration process.

Case 1:

For examining the effect of small sphere volume charge density (ρ_1) on the electrostatic interaction, we choose the volume charge density of large sphere ρ_2 = 0.5 e/nm^3, the radius of small sphere a = 8 *nm*, the radius of large sphere R = 10 *nm*. Assuming that both two nano particles are immersed in an aqueous solution of dielectric constant ε_r = 78 under a 1:1 solution with salt concentration of 10 mM equivalent to Debye screening length κ = 0.3nm^{-1}, by taking the volume charge density ρ_1 to have the following values (-5 e/nm^3,-10 e/nm^3, -15 e/nm^3).

Case 2:

For examining the effect of the dielectric constant ε_r of interacting spheres in the solution and the medium on the interaction between two nano particle spheres, we choose the volume charge densities of small sphere(ρ_1) and the large one(ρ_2) to be -5 e/nm^3, 0.5 e/nm^3, respectively. The radius of small sphere (a) and the large one(R) are to be 8 *nm*, 10 *nm*, respectively. Assuming that both particles are immersed in an

aqueous solution with 1:1 solution giving a salt concentration of 10 mM equivalent to Debye screening length $\kappa = 0.3 nm^{-1}$. By taking the dielectric constant ε_r to have the following values (70, 78, 84).

Case 3:

For examining the effect of salt concentration of a 1:1 solution having a dielectric constant $\varepsilon_r = 78$ on electrostatic interaction between two interacting spheres where the salt concentration is expressed by Debye screening length κ, we choose the volume charge density of the small sphere (ρ_1) and the large one (ρ_2) to be -5 e/nm^3, 0.5 e/nm^3, respectively. The radius of small sphere (a) and the large one(R) are taking the values 8 *nm*, 10 *nm*, respectively. We can achieve this goal by taking Debye screening length of the values (κ = 0.2 nm^{-1}, *0.3* nm^{-1}, 0.5 nm^{-1}), these values correspond to salt concentration of 3.7 mM, 10 mM and 23 mM.

In the previous three cases, we used the three stage model developed by Ohshima (*Ohshima, 2013*). The model equations describe three stages of electrostatic interaction in the three regions. The effects of electrostatic parameters on interaction were plotted as in Figure 3.2.

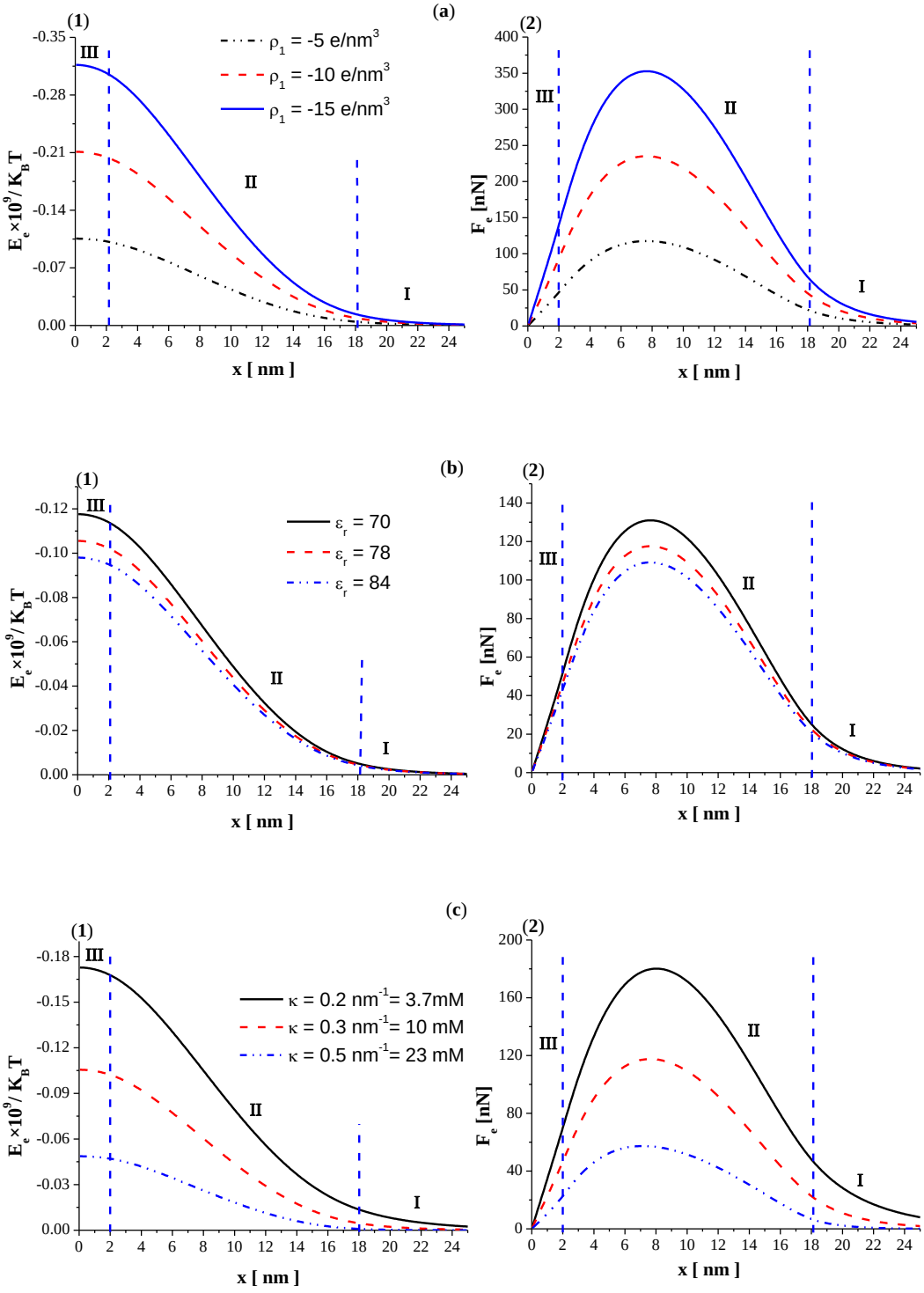

Figure 3.2: **a**) Electrostatic interaction under the effect of volume charge density of small sphere (ρ_1) **b**) Electrostatic interaction under the effect dielectric constant (ε_r) and **c**) Electrostatic interaction under the effect of salt concentration expressed in Debye screening length (κ)

Referring to Figure 3.2, it can be seen that electrostatic interaction located in three regions for the three stages, we are concerning with the second stage of interaction represented with region II located in the interval [2 *nm*, 18 *nm*], because it involves interpenetration process. The begging of interaction starts at a distance x = 18 *nm* (about to contact) and ends at a distance x = 2 *nm* (engulfing state). We found that electrostatic interaction tends to increase approximately in the first two third during the second stage till it reaches a maximum value. At this interval we can predict a maximum interpenetration. Referring to Figure 3.2a, it can be seen that electrostatic interaction in the three regions increases by increasing volume charge density distribution of small nano particle sphere (ρ_1). In Figure 3.2b, we found the electrostatic interaction increase by decreasing dielectric constant (ε_r) of interacting spheres or the medium. As a result, the curve that has a maximum electrostatic interaction is assigned to one that has a lowest material dielectric constant. This fact serves us concluding that penetration for lipid membrane that has a lowest dielectric constant is larger to be penetrated than one possessing high dielectric constant. For example, dendrimer as a nano particle has a dielectric constant around the value of 2. Each material has its specific dielectric constant electrical property. 1, 2-dimyristoyl-sn-glycero-3-phosphorylcholine (DMPC) and 1-stearoyl-2-oleoyle-sn-glycero-3-phosphocholine (SOPC) are examples of membranes materials, these two types of membrane were studied by Dietrich and Co-workers (Dietrich *et al., 1997*). Examining Figure 3.2c, it can be seen that electrostatic interaction increases by increasing Debye screening length (κ^{-1}) (decreasing salt concentration). This result serves us to predict that penetration is highest for the medium that has lowest salt concentration. Similar experimental study was done using Cryogenic Transmission Electron Microscopy (CTEM) images technique showed that salt concentration is

driven by entropy increase due to releasing counter ions in solution. When the morphology of G_2/DNA aggregates have studied in aqueous solution of 10 mM NaBr, 50 mM NaBr and 150 mM NaBr, it was found that increasing salt concentration leads to decreasing the potential interaction(*Marrink, et al.,2007*). Controlling that parameter will enable us to control electrostatic interaction as well as interpenetration.

3.4 Penetration due to electrostatic energy only

In this section, our aim requires to concentrate on the penetration, so we want to focus on the region that involves interpenetration process - region II. Taking penetration as a function of ratio $Z(r)$ where r is the ratio between the sizes of small sphere to large one (a/R) under the influence of electrostatic interaction only. This can be achieved by solving Eq. (2.13) which represents the derivative of electrostatic energy in the second stage (E_{Stage2}) with respect to penetration (z), we solved it numerically for obtaining penetration at equilibrium $Z_e(r)$. By setting the ratio r to run from 0.01 up to 1 after fixing Debye screening length $\kappa = 0.3\ nm^{-1}$ which requires 10 mM of salt concentration and also setting volume charge densities of small sphere and large one to be $\rho_1 = -2.14\ e/nm^3$, $\rho_2 = 0.5\ e/nm^3$, respectively. Assuming both two interacting spheres immersed in monovalent aqueous solution (1:1 salt solution) with dielectric constant $\varepsilon_r = 78$. See Figure 3.3.

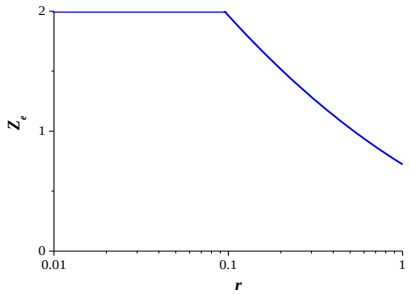

Figure 3.3: Penetration as a function of ratio $Z_e(r)$ under the effect of electrostatic energy E_{Stage2} only, with Debye screening length $\kappa = 0.3\ nm^{-1}$(10 mM 1:1 solution), small sphere volume charge density $\rho_1 = -2.14\ e/nm^3$, large sphere volume charge density $\rho_2 = 0.5\ e/nm^3$ of interacting spheres and dielectric constant $\varepsilon_r = 78$.

Referring to Figure 3.3, the penetration process that could be accompanied with wrapping process has been studied. For very small particle it is totally penetrated while for large ones, particle penetration is slowing down the value 2, particle could be wrapped. We have found that penetration at equilibrium Z_e decreases at large ratios under electrostatic interaction in region II while at very small ratios the penetration is totally complete (Z_e=2) which represents the engulfing state. The effect of dielectric constant and volume charge densities of two spheres totally disappeared, while the effect of salt concentration given in terms of Debye screening length has incomplete effect because some terms located in the phase of the equation. Mathematically, studying penetration under electrostatic energy only makes some parameters to disappear during making mathematical operation like derivation. This reason makes taking electrostatic energy to study penetration is not complete. Physically this fact could be compared with studying penetration under the line curvature energy (*Dietrich et al., 1997*). This is impossible without taking adhesion energy and bending energy as line curvature energy resulted from perturbation from adhesion and bending energies. That is why taking adhesion and bending energies to study electrostatic energy (interaction initiator) is unavoidable. The spheres must keep in contact to see the effects of electrostatic interaction. Table 3.1 gives the penetration values Z_e for different ratios r under effects of electrostatic interaction only.

Table 3.1: Penetration Z_e values at different ratios r under electrostatic energy (E_{Stage2}) only

Ratio r	Panetration Z_e
0.1	1.96256140
0.2	1.51624921
0.3	1.28460146
0.4	1.13336243
0.5	1.02338037
0.6	0.93828722
0.7	0.86963983
0.8	0.81261024
0.9	0.76417375
1	0.72232470

3.5 Penetration under the total energy (Adhesion, Bending, Electrostatic)

In section 3.4, we have studied the penetration as a function of ratio $Z_e(r)$ under the influence of electrostatic energy that concentrates on the second stage only. In this section, we shall study the penetration under total energy described by Eq. (2.28). Taking the two interacting nano particle spheres such as the small sphere has a radius of 8 *nm* and the large one has a radius of 10 *nm* and both spheres having volume charge densities ρ_1 = -5 e/nm^3, ρ_2 = 5 e/nm^3, respectively. The spheres are assumed to be immersed in aqueous monovalent solution of a salt concentration equals to 10 mM gives a Debye screening length κ = 0.3 nm^{-1} having a dielectric constant ε_r = 78 (*Ohshima, 2013*). The assumed relative excess area ε_{ab} was taken to be -0.005 and the adhered substrate area density A is 0.001 J/m^2. By substituting these values in Eq. (2.28), then making differentiation as in Eq. (2.32) and solving the equation numerically. We calculated the sum of adhesion and bending energies E_{ab} as well as the correspondence force F_{ab} as in Eq. (2.25) and its derivative. Also for total energy using Eq. (2.28) and total force using Eq. (2.30). The obtained results are shown in Figure 3.4.

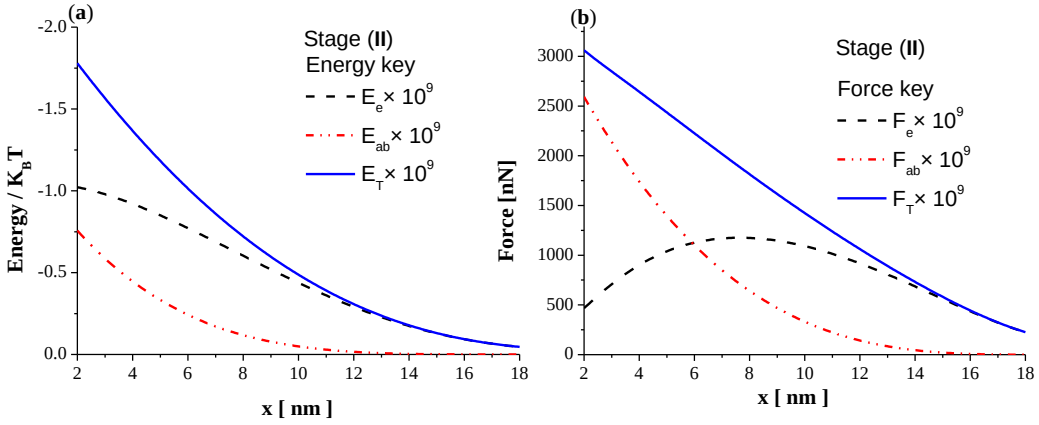

Figure 3.4: **a**) Total energy $E_T(x)[K_BT]$, electrostatic energy $E_e(x)[K_BT]$ and the sum of adhesion and bending energies $E_{ab}(x)[K_BT]$ **b**) Total force $F_T(x)[nN]$, electrostatic force $F_e(x)[nN]$ and the sum of adhesion and bending forces $F_{ab}(x)$ $[nN]$ for two spheres of radii a = 8 *nm*, R = 10 *nm* carrying volume charge densities ρ_1 = -5 e/nm^3, ρ_2 = 5 e/nm^3, respectively. Dielectric constant ε_r = 78, adhered area density A = 0.001 J/m^2, relative excess area ε_{ab} = -0.005 and Debye screening length κ = 0.3nm^{-1}(10 mM 1:1 solution) in both two cases in stage II.

When we take the radius of small sphere a = 8 *nm* and the large one R = 10 *nm*, the interpenetration process is strictly located in the interval [2 *nm*, 18 *nm*]. As it could be seen from Figure 3.4, the influence of the electrostatic energy (E_e) surpasses the sum of adhesion and bending energies combined with each other (E_{ab}) as a result, the total free energy (E_T) of the interacting system would also increase by adding electrostatic energy term. It is clear that the force resulted from adhesion and bending energies (F_{ab}) is less than the electrostatic force (F_e) in the first two third of second stage that starts at distance x =18 *nm* (nearly being touch) and continues to increase till it ends at distance x =2 *nm* (engulfing stage). The resultant total force (F_T) also increases and no effect of electrostatic force without the adhesive and bending forces (adhesive and bending forces work as initiator for interaction) can be observed. This picture of comparison is similar to that one that was done by Dietrich model when they studied the penetration under adhesion, bending and curvature forces, they could not study the curvature force alone (even if it was negligible, its contribution 10^{-3} form the total

energy) (*See Appendix* A**;** *Dietrich et al., 1997*). The increase of the energy value, the accompanied force also affects the penetration to increase dramatically. This fact appears through curves comparison between penetration values with and without electrostatic interaction as shown in Figure 3.5.

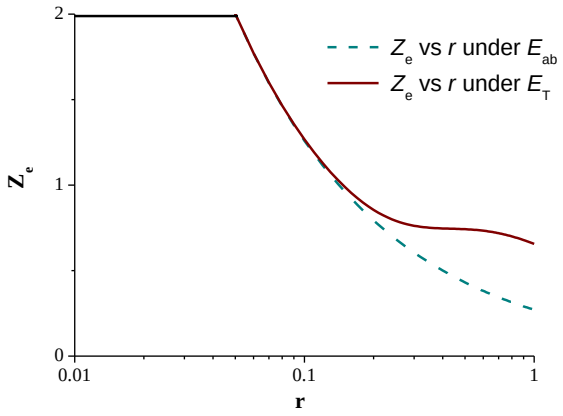

Figure 3.5: Comparison study for penetration Z_e versus ratio r with and without electrostatic energy effect where adhered area density A= 0.001 J/m^2 and a relative excess area ε_{ab} = 0, volume charge densities ρ_1 = -2.14 e/nm^3, ρ_2 = $0.5e/nm^3$ for small sphere and large one, respectively. Debye screening length κ = 0.3 nm^{-1}(10 mM 1:1 solution) and dielectric constant ε_r = 78.

The results illustrated in Figure 3.5 show that increasing the value of energy by adding the electrostatic energy term to adhesion and bending energies terms would resulted in increasing in penetration. The maximum value of for penetration curve $Z_e(r)$ occurs at the intersection point with the horizontal line described by the equation Z_e=2 which represents the upper limit for penetration. At values (r) below that point, the particle is totally penetrated into the large particle sphere to reach the engulfing state (*Ohshima, 2013*). At ratios greater than the intersection point, the small particle sphere is partially penetrated into the large particle sphere. Two accompanied interactions may occur for the small particle, namely, wrapping and penetration. Penetration occurs at small ratios and tends to decrease as the ratio is increasing up to reach the ratio 1. Eventually, small particle starts to grow up gradually (at high ratios) penetrations

tends to slow down (less than 2) and the ability for wrapping particle tends to increase rather than penetrating(*Dasgupta et al., 2013*). It is clear from Figure 3.5 that electrostatic energy term increases the total force. This increase resulted from increasing the attractive electrostatic force between two interacting nano particles. The increase in force would also lead to increase penetration dramatically. By comparing the results of the penetration with electrostatic energies and without electrostatic energy term (adhesion and bending energies only), a noticeable difference is reported in penetration (Δ **(Z_e)** $\uparrow$) which is very high at large ratios, increase is due to the amount of the charge the particles may carry. This result is made consisted with study that was done by Dietrich and Co-workers for two neutral interacting nano particles (*Dietrich et al., 1997*). All results are illustrated in Table 3.2 and illustrated in Figure 3.5.

Table 3.2 Difference in penetration **(Δ (Z_e) $\uparrow$)** before adding the electrostatic term (*Dietrich et al., 1997*) and after adding electrostatic term.

Ratio r	Penetration Z_s under Adhesion + Bending $\rightarrow E_{ab}$	Penetration Z_s under Adhesion + Bending + Electrostatic $\rightarrow E_T$	Increase in Penetration $\Delta(Z_e)\uparrow$
0.1	1.25992105	1.26729981	0.00737876
0.2	0.79370053	0.85513855	0.06143802
0.3	0.60570686	0.76224537	0.15653851
0.4	0.50000000	0.74659742	0.24659742
0.5	0.43088694	0.74218930	0.31130236
0.6	0.38157141	0.73345737	0.35188596
0.7	0.34430604	0.71885752	0.37455148
0.8	0.31498026	0.70001527	0.38503501
0.9	0.29119349	0.67876402	0.38757054
1	0.27144176	0.65650270	0.38506094

If we look at Table 3.2, we can see for very low ratios (< 0.1), the small nano particle reachs the engulfing state in the existence of electrostatic term faster than without electrostatic term (neutral particles). Solving Eq. (2.28) that represents total free energy of the system under the sum adhesion energy, bending energy and electrostatic energy numerically, we can check the impacts of different parameters affecting

penetration. process. Studying each parameter alone allow us to control the process of interpenetration, we will discuss each parameter as in the following subsections.

3.5.1 The effect of relative excess area (ε_{ab})

In this subsection, we want to investigate the impacts of relative excess area parameter (ε_{ab}) which represents the relative excess area at the large sphere. This goal could be achieved by taking total energy derivative with respect to penetration and finding extreme values ($\frac{dE_T}{dz} = 0$) as in Eq. (2.32). Assuming both two spheres having volume charge densities ρ_1 = *-2.14 e/nm*^{3} for small sphere, ρ_2 = *0.5 e/nm*^{3} for large one, immersed in aqueous solution of dielectric constant ε_r = 78 with a 1:1 salt of concentration equals to 10 mM gives a Debye screening length κ = 0.3 *nm*$^{-1}$ with adhered substrate area density A = 0.001 *J/m*^{2}. Then fixing all variables and taking ε_{ab} to have the following values (-0.005,-0.0025,0,0.0025,0.005,0.01) and then solving for penetration (z) numerically by setting ratio (r) to run from 0.01 up to 1, the results of penetration function $Z_e(r, \varepsilon_{ab})$ can be calculated. The results are plotted in Figure 3.6.

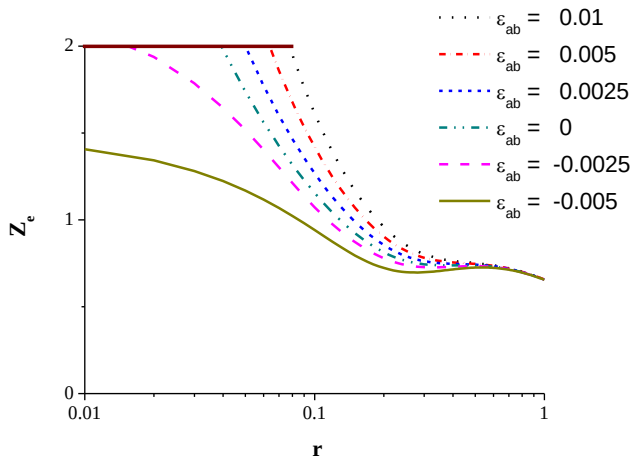

Figure 3.6: The penetration value Z_e versus ratio r for two interacting spheres having volume charge densities ρ_1 = *-2.14 e/nm*^{3}for small one, ρ_2 = *0.5 e/nm*^{3} for large one, dielectric constant ε_r = 78, Debye screening length κ = 0.3 *nm*$^{-1}$(10 mM 1:1 solution) and adhesive energy density A = 0.001 *J/m*^{2} with a varies relative excess area ε_{ab}.

Figure 3.6 shows that penetration (Z_e) increases by increasing the value of relative excess area ε_{ab}. Such increase is resulted from enlarging the exposed area for electrostatic interaction by increasing relative excess area (ε_{ab}). Also, Z_e reaches a maximum value at very small ratios (ratio $r \rightarrow 0$) where the penetration is totally complete (horizontal line Z_e=2) which represents the engulfing state for those curves that doesn't cut penetration Z_e axis. A general observation, penetration decreases by increasing the ratio which was obtained by Dietrich-Coworkers study(*Dietrich et al., 1997*). This is true after adding electrostatic term, some turning points exist during the balances between three forces adhesion, bending and electrostatic. Since distribution may be affected during penetration process i.e.; changed from sphere to ellipsoidal or rod especially we are dealing with nano particles or a number of interacting particles. At very high ratio the penetration is so much close which is explained by small charge neutralization, while at very small ratio the curves are apart where the dominant force is electrostatic (See section 3.5). It is clear that penetration with the existence of electrostatic energy is larger than with adhesion and bending energies through comparing the Figures 3.6 and 1.10a. Hence, the effect of relative excess area still very small, the jumps in penetration for each value occurred resulted from electrostatic energy term that has its own parameters affecting the process. Table 3.3 gives penetration under the total energy at fixed relative excess area $\varepsilon_{ab} = 0$.

Table 3.3: Penetration values Z_e for different ratios r for two interacting spheres having volume charge densities ρ_1 = *-2.14 e/nm*^{3} for small sphere, ρ_2 = *0.5e/nm*^{3} for large one, dielectric constant ε_r = 78, Debye screening length κ = 0.3 *nm*$^{-1}$(10 mM 1:1 solution), and adhesive energy density A= 0.001 *J/m*^{2}.

Ratio	Penetration
r	Z_e
0.1	1.26000722
0.2	0.79450255
0.3	0.60837697
0.4	0.50596337
0.5	0.44161583
0.6	0.39840522
0.7	0.36831841
0.8	0.34691442
0.9	0.33145528
1	0.32013739

By comparing Table 3.3 with column two in Table 3.2, we can see, for example, at ratio r = 0.1, the data appears as in increase in penetration difference ((Δ **(Z_e)** ↑) by 0.00008617. This difference is too small and natural for small ratio. Similar results were obtained for high ratios the difference is still small, for example, at ratio r = 1, penetration difference ((Δ **(Z_e)** ↑) of 0.04869536. This result indicates that relative excess area effect is so small compared with electrostatic parameters effects (*Dietrich et al., 1997*).

3.5.2 The effect of adhered area substrate density (A)

In this subsection, we want to investigate the impacts of adhered area substrate density parameter A which represents the contact area density energy. This goal could be achieved by taking finding the extreme values of total energy as in Eq.(2.28) by differentiating with respect to penetration as in Eq.(2.32) ($\frac{dE_T}{dz} = 0$) . Assuming both two spheres having volume charge densities ρ_1 = *-2.14 e/nm*^{3} for small sphere, ρ_2 = *0.5 e/nm*^{3} for large one, respectively, Spheres are assumed to be immersed in aqueous solution of dielectric constant ε_r = 78 with a 1:1 salt of concentration equals to 10 mM

gives a Debye screening length κ = 0.3 nm^{-1} with relative excess area(ε_{ab} = 0). After that, values of A are chosen to be (0.0001, 0.0002, 0.0005, 0.001, 0.002, 0.005) J/m^2 and then solving for penetration function $Z_e(r, A)$ numerically by setting ratio (r) to run from 0.01 up to 1. The results were plotted in Figure 3.7.

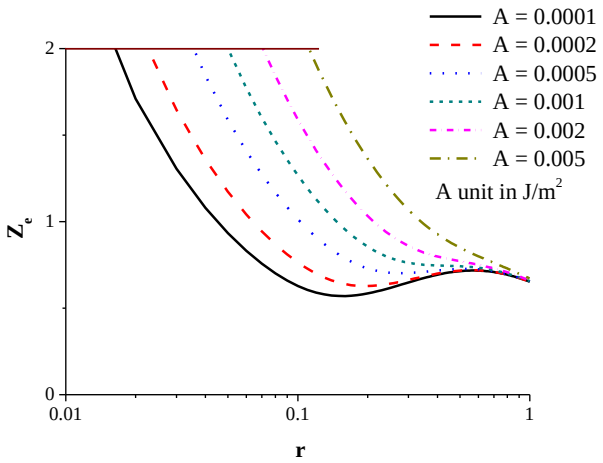

Figure 3.7: The penetration value Z_e versus ratio r for spheres having volume charge densities ρ_1 = *-2.14 e/nm*^{3} for small sphere, ρ_2 = *0.5 e/nm*^{3} for large one, dielectric constant ε_r = 78. Debye screening length κ = 0.3 nm^{-1}(10 mM 1:1 solution) and relative excess area ε_{ab} = 0.

Comparing between Figure 3.7 and Figure 1.10b that represent the penetration with and without the existence of electrostatic energy at constant A parameter. It is similar results were obtained for as relative excess area parameter except some turning points for each curve result from the balance between three forces (*Dietrich et al., 1997*). At the ratio r < 0.1 it is same as figure 1.14b, but at ratio r > 0.1 approximately penetration tends to rise, this fact is due to electrostatic interaction for the area exposed between negative and positive charges that speeds up the penetration. By looking at Figure 3.7, we can notice that penetration (Z_e) increases by increasing the value of adhered area substrate density parameter A resulted from enlarging the electrostatic interaction that the area exposed, Z_e is found to reach a maximum value at very small ratios (ratio $r \rightarrow 0$), where the penetration is totally complete at the horizontal line (Z_e=2) that represents the engulfing state for those curves that doesn't cut Z_e axis. Also,

penetration decreases by increasing the ratio. At very high ratio the penetration curves at different values of A are so very close. This can be explained on the basis of small charge neutralization (electrostatic force surpasses adhesion and bending forces). The behavior at very small ratio the curves are apart where the dominant force is electrostatic (See section 3.5). It is clear that penetration with the existence of electrostatic energy is larger than with adhesion and bending energies still true under the effect of that parameter, this fact is consistence with the fact that was obtained through studying two cylindrical soft particles (*Ohshima, 2010*).

3.5.3 The effect of volume charge density (ρ_1)

In this subsection, we want to investigate the impacts of volume charge density of the small interacting particle sphere (ρ_1) while keeping the volume charge density of the large one being constant (ρ_2 = *0.5 e/nm*^{3}). This goal could be achieved by taking total free energy Eq. (2.28) and differentiate it with respect to penetration z for finding extreme values ($\frac{dE_T}{dz} = 0$) as in Eq. (2.32). Assuming ρ_1 have the following values (*-0.5,-1.5,-2.5,-10,-50)* e*/nm*^{3}. Both spheres are assumed to be immersed in aqueous solution of dielectric constant ε_r = 78 with a 1:1 salt of concentration equals to 10 mM gives a Debye screening length κ = 0.3 *nm*$^{-1}$ with relative excess area (ε_{ab} = 0) and adhered area substrate density parameter (A = 0.001 *J/m*^{2}) and then solving Eq. (2.32) for penetration (*z*) numerically by setting ratio *r* to run from 0.01 up to 1. Result are illustrated in Figure 3.8 and illustrated in Table 3.4.

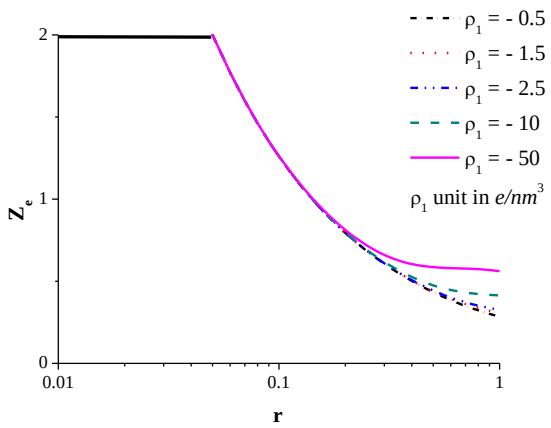

Figure 3.8: The penetration value Z_e versus ratio r for two interacting spheres carrying volume charge densities ρ_1 for small sphere, ρ_2 = *0.5e/nm*^{3} for large one, dielectric constant ε_r = 78. Debye screening length κ = 0.3 *nm*$^{-1}$(10 mM 1:1 solution), relative excess area ε_{ab} = 0 and adhered substrate area density A= 0.001 *J/m*^{2}.

Table 3.4: Penetration Z_e values for different ratios r for two interacting spheres of radius a carrying volume charge densities ρ_1 and a large sphere carries a volume charge density ρ_2 = *0.5e/nm*^{3}, dielectric constant ε_r = 78, Debye length κ = 0.3 *nm*$^{-1}$(10 mM 1:1 solution), relative excess area ε_{ab} = 0 and adhered substrate area density A= 0.001 *J/m*^{2}.

ρ_1[e/nm^3]	-0.5	-1.5	-50
Ratio r	Penetration Z_e		
0.1	1.25994118	1.25998145	1.26192798
0.2	0.79388815	0.79426296	0.81180170
0.3	0.60633379	0.60758202	0.66061126
0.4	0.50141122	0.50420067	0.60475156
0.5	0.43345966	0.43848269	0.58600451
0.6	0.38568590	0.39357483	0.58012386
0.7	0.35032282	0.36158425	0.57720687
0.8	0.32322480	0.33820286	0.57359926
0.9	0.30194556	0.32081183	0.56819978
1	0.28492978	0.30769654	0.56091945

In our study, we replacing the two neutral interacting spheres studied by Dietrich and Co-workers (*Dietrich et al., 1997*) with charged ones. Significant change in penetration occurs. This change is a result of increasing total energy of interacting system by adding electrostatic energy. This increase will enhance interpenetration, that increase was a result of increasing the volume charge density of the interacting particle. Through increasing the volume charge density, the attractive force makes the interpenetration between spheres easy. As in the previous, the horizontal line Z_e=2

forms the high upper limit for penetration (totally complete penetration). It represents the engulfing state, for the small ratios, the nano particles are totally penetrated when the particle tends to grow gradually the penetration starts to decrease less than the value 2, for those ratios possessing penetration less than 2, it is exposure to be wrapped around large one(*Dasgupta et al., 2013*). Moreover, penetration decreases by increasing the ratio as it was done in Dietrich model (*Dietrich et al., 1997*). Some turning points exist resulted from changes for spheres shape and size through interaction due to the electrostatic interaction. At a very small ratio the curves are very close and penetration is very high where the dominant force is electrostatic because of the negligible size of small sphere. But at very high ratios the curves are distinguishable (apart from each other). It is clear that penetration with the existence of electrostatic energy is larger than with adhesion and bending energies through comparison.

This study could be approximately compared with dendrimer-DNA complexation which is driven by electrostatic interaction. For example, wrapping process increases by increasing dendrimer generation through increasing amine groups that carry charge on their outer surface (*Welch and Muthukumar, 2000*). Our study for penetration process under the effect of volume charge density was verified experimentally using Inductively Coupled Plasma Mass Spectroscopy (ICM-MS) technique through investigating the adsorb process for neutral and negatively particles by cell membrane surface. They found that neutral and negatively charged nano particles adsorbed much less on negatively cell membrane surface also they showed lower level of internalization compared with positively charged particles (*Ayush and Francesco, 2009*). We found that charge has a great influence on penetration process, that factor enables us to control penetration.

3.5.4 The effect of dielectric constant (ε_r)

In this subsection, we want to investigate the impacts of the dielectric constant ε_r of the two interacting spheres and the medium too. This goal could be achieved by taking total free energy Eq. (2.28) and differentiate it with respect to penetration as in Eq. (2.30). Then finding the extreme values ($\frac{dE_T}{dz} = 0$). Assuming both two spheres having volume charge densities ρ_1 = *-2.14 e/nm*^{3} for small sphere and ρ_2 = *0.5 e/nm*^{3} for the large one immersed in aqueous monovalent solution of salt concentration equals to 10 mM gives a Debye screening length κ = 0.3 *nm*$^{-1}$ with relative excess area ε_{ab} = 0 and adhered area substrate density (A = 0.001 *J/m*^{2}) . Taking ε_r to be (84, 78, 70 and 2) and substituting the rest of parameters then solving Eq. (2.30) numerically for penetration (z) by setting ratio (r) to run from 0.01 up to 1. The data are plotted as in Figure 3.9.

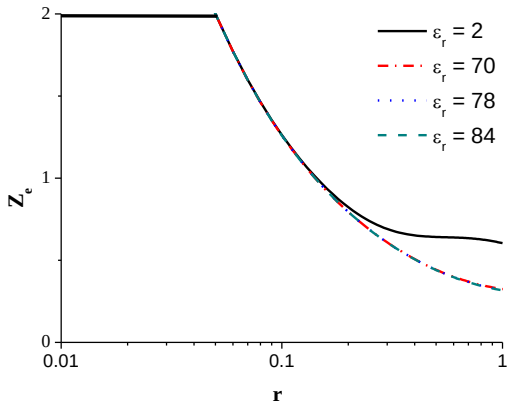

Figure 3.9: The penetration value Z_e versus ratio r with spheres charge densities ρ_1 = -2.14 *e/nm*^{3}, ρ_2 = *0.5 e/nm*^{3}, respectively. Adhered substrate area density A= 0.001 *J/m*^{2}. Debye length κ = 0.3 *nm*$^{-1}$ (10 mM 1:1 solution) and relative excess area ε_{ab} = 0 with a varies dielectric constant ε_r.

Looking at Figure 3.9, it was found that increasing the total energy of system, by selecting the material with lowest dielectric constant, penetration at equilibrium (Z_e) increases by decreasing the value of dielectric constant (ε_r) of the two interacting spheres (it depends on the material of interacting spheres). It reaches its maximum

value at a very small ratios (ratio $r \rightarrow 0$) where the penetration is totally complete (Z_e=2). So decreasing the dielectric constant will increase the electrostatic energy and hence affects by decreasing the total energy that affects the penetration to increase dramatically. This electrical property differs by different material, which enables us to control the process of interpenetration. Dietrich model (*Dietrich et al., 1997*) was based on two types, 1-stearoyl-2-oleoyle-sn-glycero-3-phosphocholine (SOPC) and 1, 2-dimyristoyl-sn-glycero-3-phosphorylcholine (DMPC) membranes, their dielectric constants ≈ 2.1, 4.2, respectively. Each type of membrane differs in that property. We found that the material with the lowest dielectric constant may lead to be high penetrating. Table 3.5 shows the penetration variation with dielectric constant ε_r.

Table 3.5: Penetration values Z_e for different ratios r for two interacting spheres, the small sphere has volume charge density ρ_1 = -2.14 e/nm^3, and a large one has a volume charge density ρ_2 = $0.5e/nm^3$, Debye screening length κ = 0.3 nm^{-1}(10 mM 1:1 solution), relative excess area ε_{ab} = 0 and adhered substrate area density A = 0.001 $J/m^2$with a varies dielectric constant ε_r.

ε_r	2	70	78	84
Ratio r	Penetration Z_e			
0.1	1.26326366	1.26001706	1.26000722	1.26000106
0.2	0.82322469	0.79459405	0.79450255	0.79444535
0.3	0.69068198	0.60867995	0.60837697	0.60818738
0.4	0.65161917	0.50663242	0.50596337	0.50554394
0.5	0.64211833	0.44279702	0.44161583	0.44087311
0.6	0.63889029	0.40020923	0.39840522	0.39726616
0.7	0.63443109	0.37080455	0.36831841	0.36674073
0.8	0.62697799	0.35008922	0.34691442	0.34488848
0.9	0.61666740	0.33528196	0.33145528	0.32899928
1	0.60417072	0.32455046	0.32013739	0.31728900

3.5.5 The effect of salt concentration in terms of Debye length (κ)

We want to investigate the impacts of the salt concentration in the expressed intern of Debye screening length (κ). This goal could be achieved by taking total free energy Eq.(2.28) and differentiate it with respect to penetration as in Eq.(2.30) . Then finding

extreme values ($\frac{dE_T}{dz} = 0$). Assuming both two spheres having volume charge densities ρ_1 = *-2.14 e/nm^3* for small sphere and ρ_2 = *0.5 e/nm^3* for large one immersed in aqueous monovalent solution with relative excess area (ε_{ab} = 0) and adhered area substrate density (A = 0.001 *J/m^2*). After that fixing all variables and making κ to be assigned the values (0.3, 1.05 and 1.28) *nm^{-1}* that corresponds to salt concentration values (10,100,150) mM, respectively. Solving Eq. (2.30) for penetration (*z*) numerically by setting ratio (*r*) to run from 0.01 up to 1. The data are plotted as in Figure 3.10.

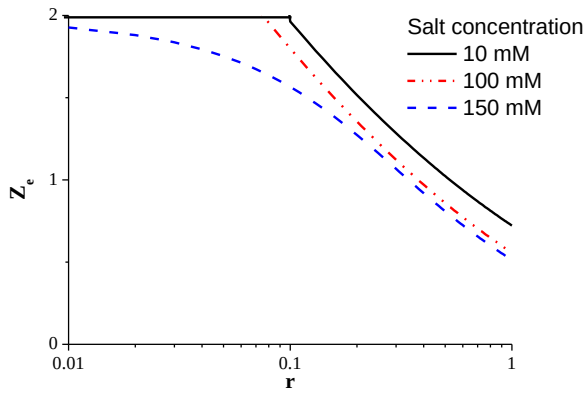

Figure 3.10: The penetration value Z_e versus ratio *r* for two interacting spheres having volume charge densities ρ_1 = -2.14 *e/nm^3* for small sphere, ρ_2 = 0.5 *e/nm^3* for large one, relative excess area ε_{ab} = 0, adhered area density A= 0.001 *J/m^2* with a varies mono salt concentration having dielectric constant ε_r =78.

Referring to Figure 3.10, high penetration occurred at low Debye length (κ^{-1}) that corresponds to low salt concentration where Debye length represents the double layer thickness. It has great importance in colloid stability and for that matter in flocculation. It controls the range of double layer interaction. For those curves that doesn't cut penetration Z_e axis it is bounded with maximum penetration value (Z_e=2). It is completely penetrated, for ratios r approaching near zero. The thickness of double layer is controlled by concentration and valences of ions in solution. High concentration of ions (high ion strength) in the medium generally results to increase the

double layer thickness that affects particle motion through penetration process i.e. the concentrations(10 mM ,100 mM and 150 mM) corresponds to Debye screening length (κ^{-1}) values (3.3 ,0.95 and 0.78) *nm* respectively . So increasing double layer thickness would decrease penetration. Penetration interaction when compared to wrapping process, the study showed that increasing the pH degree (from acid to base environment), will resulted in decreasing the wrap process (*Luo et al., 2002*). Through solving Eq. (2.30) numerically, the calculation results are summarized in Table 3.6.

Table 3.6: Penetration values Z_e for different ratios r for two interacting spheres having volume charge densities ρ_1 = -2.14 e/nm^3 for small sphere, ρ_2 = 0.5 e/nm^3 for large one, relative excess area ε_{ab} = 0, adhered area density A= 0.001 J/m^2 with varies 1:1 of a salt concentration solution having dielectric constant ε_r =78.

Salt concentration	10 mM	100 mM	150 mM
Ratio r	Penetration Z_e		
0.1	1.96256140	1.79944403	1.56511407
0.2	1.51624921	1.35485921	1.27348489
0.3	1.28460146	1.12282238	1.06697861
0.4	1.13336243	0.97046737	0.91875798
0.5	1.02338037	0.85947129	0.80902867
0.6	0.93828722	0.77359726	0.72430607
0.7	0.86963983	0.70449205	0.65637357
0.8	0.81261024	0.64731043	0.60038089
0.9	0.76417375	0.59900098	0.55326795
1	0.72232470	0.55752306	0.51298528

From Table 3.6, it is noticeable by increasing the salt concentration in the interaction environment will lead to release ion, as the ion become more strength in solution, the interpenetration process is impeded. So controlling the salt concentration in the environment enables us to control the process of particle penetration.

Chapter Four

Conclusions and Future work

4.1 Conclusions

After completing our study that was based on comprising the model for electrostatic interaction between two soft porous interpenetrating spheres by Ohshima (*Ohshima, 2013*) and the analytical study that was produced by Dietrich and Co-workers for neutral particles (*Dietrich et al., 1997*). We modified such model by constructing a new equation for total free energy of interacting system through comprising process, and then we solved the total free energy equation numerically for investigating the electrostatic parameters. After studying the new total free energy of the system, it was found that adding electrostatic energy into adhesion and bending energies causes to increase total free energy, total free force and interpenetration. We also found that charged particle penetrated larger than neutral ones. The dramatic increase in interpenetration is due to the to effects of electrostatic parameters, taking into account the system is isolated from other effects like viscosity, thermal energy, etc. as well line curvature energy which is assumed to be discarded, since its contribution is negligible in Dietrich model study. We obtained that electrostatic interaction surpasses adhesion and bending interaction in the first two third of interaction (mainly second stage of Ohshima model). The new significant parameters that were investigated came from the electrostatic energy term, namely, the charge of small interacting sphere expressed as a volume charge density (ρ_1), the dielectric constant of the medium (ε_r) as well spheres in addition to salt concentration. Mentioned parameters have a varied effect. We found that the volume charge density of small interacting sphere would increase the electrostatic energy that reflects an increase in total free energy which causes the interpenetration process to increase. Relevant to dielectric constant of medium, we found that decreasing the dielectric constant will cause an increase to total free energy

which reflects an increase in interpenetration process. Salt concentrations were found to decrease penetration due to barriers resulted form the path which is crowded with high ion concentration, through loading specific values for electrostatic parameters enables us to control the interpenetration in different applications. The penetration of nanoparticles have important role that could be applied in genetics and molecular mechanism in medicine and drug responses. Also charged nanoparticles provide great opportunities to explore the potential of using nanomaterial as vehicles for the delivery of DNA, proteins and nucleus. Charged nanoparticles may be faster than neutral nanoparticle during cancers cell attack. Therefore, in this way, we can speed up the process of interpenetration and the result of treatment success reach faster.

4.2 Future work

Extending Ohshima's model with other parameters

The proposed model by Ohshima could be modified by adding some parameters related to the nature of interaction medium and the soft particles, like the blood viscosity, the turbidity, the permittivity, and the shape of two interacting nano particles and their nature, etc., to obtain reliable results which lead to new design for drugs applied for human cells.

Extending Ohshima's model to be on number N of interacting particles

In principle, the proposed three-stage model summary is describing, studying the penetration and calculating the interactions between two soft charged porous particles. But it be could enlarged to accommodate N soft charged porous interpenetrating particles data. N particle data considerably increases the difficulty of the estimations and calculations for N particles effects. Ohshima's three-stage model has not yet been implemented for the interaction of N interpenetrating particles.

Appendix A

Contact line energy (*Dietrich et al., 1997***)**

The vesicle radius is very large ($R >> a$) in picture. In the region of the contact line, the membrane is supposed to follow a toroidal shape, between points *A* and *C* in the cross-section is the true membrane-sphere contact point. We denote ρ the radius of the tore cross section. The angle α defined in figure simply related to the contact angle by $\theta = \pi - \alpha$.

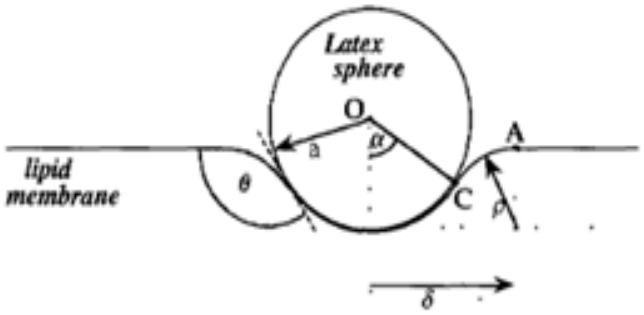

Figure A: Bending membrane near to the membrane-solid sphere contact line

Taking the limit $R >> a$, z = 1-cos α was only variable in the energy of the system. Now we have to handle two variables, namely α and ρ, the goal of this appendix is estimate the value of ρ at equilibrium and the importance of the toroidal portion of the membrane in the total energy. We calculate bending energy E_b, adhesion energy E_a and line energy E_l. We have:

$$S_a = 2\pi a^2(1 - cos\alpha) \qquad (A.1)$$

$$S - S_0 = S_a + S_T - \pi\delta^2 - 4\pi R^2\varepsilon_{ab} \qquad (A.2)$$

S_T is the surface area of the above defined tore portion and

$$\delta = (a + \rho)sin\,\alpha \qquad (A.3)$$

is the distance between *A* and the symmetry axis. S_T is given by

$$S_T = 2\pi[(a + \rho)\rho\alpha sin\,\alpha - (1 - cos\alpha)\rho^2\,] \qquad (A.4)$$

Equations (Eq. (A.1) - Eq. (A.4)) allow us to calculate $E_a + E_b$, the line energy E_l is due to the curvature of the membrane in the contact region. The general expression of the curvature energy involves the constant K_c, K_a (mean curvature elasticity and Gaussian curvature elasticity) and is rather complex in the geometry of interest. Fortunately it simplifies considerably if we assume $\rho << \delta$. Actually, we expect this condition to be satisfied if the sphere size is not too small and if the adhesion energy is large enough to produce a significant penetration. Indeed, this is so in our experiments, and we will verify that our results are consistent with this view. The simplification leads to

$$E_l = E_c \cong k_c \frac{S_T}{\rho^2} \tag{A.5}$$

From the explicit expressions of the surface area, we find

$$E_b \cong k_a \frac{a^4}{8R^2}\left[(1-cos\alpha)^2 + 2\frac{\rho}{a}\left(cos\theta^2 - 1 + \theta sin\theta\right) - 4\varepsilon_{ab}\left(\frac{R}{a}\right)^2\right] \tag{A.6}$$

$$E_a = -2\pi A a^2(1-cos\alpha) \tag{A.7}$$

$$E_l \approx 2\pi k_c \left(\frac{a}{\rho}\right)\alpha\, sin\alpha \tag{A.8}$$

Minimization of $E_a + E_b + E_l$ as a function of ρ leads to:

$$\frac{a^2}{\rho^2} = \frac{k_a}{k_c}\frac{a^4}{4R^2}\frac{cos\alpha^2 - 1 + \alpha\sin\alpha}{\alpha\sin\alpha} \tag{A.9}$$

Thus we estimate

$$\rho \approx \frac{2R}{a}\sqrt{\frac{k_c}{k_a}} \tag{A.10}$$

with $R = 30\mu m$, $a = 8\mu m$, $k_c = 4 \times 10^{-13}\, erg/cm^2$, $k_a = 200\ erg/cm^2$, we find $\rho \approx 5\ nm$, a value on the order of the membrane thickness, i.e. near the physical lower limit of ρ. This result is obviously consistent with our assumption that $\rho << a$. ρ can be expressed as a function of the membrane tension:

$$\rho \approx \sqrt{\frac{k_c}{\sigma}} \tag{A.11}$$

in agreement with Evans estimate (*Dietrich et al., 1997*). To estimate the importance of line energy in the total energy of the system, we regard E_l as a perturbation of E_a + E_b. The minimum value of the unperturbed E_a + E_b is equal $\frac{-3\pi}{8} k_c a^4 \frac{1}{R^2}$ (for ε_{ab}= 0). Then, using Eq. (A.10) and Eq. (A.11), we find:

$$\frac{E_l}{E_b+E_a} \approx \frac{8}{3}\frac{R}{a^2}\sqrt{\frac{k_c}{k_a}} \qquad (A.12)$$

With the same numerical values as before, the above ratio is found $\approx 10^{-3}$ thus, the line energy is negligible in our conditions. This would not be true with much smaller spheres. With the same values of the vesicle radius, we find a cross over size of about 0.1 μm.

Appendix B

Ohshima three stage model (*Ohshima, 2013*)

A three-stage model of the electrostatic interaction between two charged interpenetrating charged spherical soft particles without the particle core (space-charged porous spheres) in an electrolyte solution in three states (i) interaction before contact of the two spheres, (ii) partial interpenetration, and (iii) full interpenetration, i.e., engulfing of one sphere by the other. This is an extension of the work of Dahnert and Rodenbeck (*Dähnert and Rödenbeck, 1994*), who considered the interaction between interpenetrating vesicle-like surface-charged particles, to the case of the interaction of space-charge porous spheres. Analytic expressions for interaction energy and force between two interpenetrating weakly charged porous as a function of particle separation are derived for the respective stages on basis of the linearized Poisson-Boltzmann equations for electric potential distribution .Soft particles, which are hard particles covered with an ion-penetrable surface layer of polyelectrolytes, can be a model for biological cells. Electrostatic interaction between soft particles is quite different from those for hard particles without surface structures in that the electrostatic interactions between soft particles are governed by their space-charges distributed within the particles or Donnan potentials.

Poisson-Boltzmann equations for two interacting charged porous spheres

Consider two charged porous spheres of radii R and carrying fixed charges of constant volume densities ρ_2 and ρ_1, respectively. At separation x between their centers O_1 and O_2 in an electrolyte solution containing N ionic species with valence z_i and bulk concentration (number density) n_i (i = 1, 2 ...N) (in units of) m^{-3} in three stages as shown in Figure B, that is,

(i) Interaction before contact (See Figure B.1).
(ii) Interpenetration (See Figure B.2).
(iii) Engulfing (See Figure B.3).

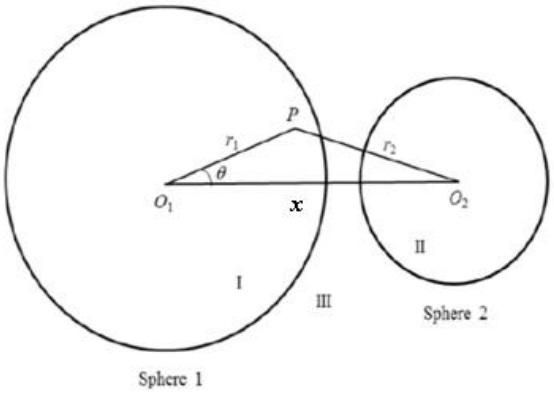

Figure B.1: Interaction before contact

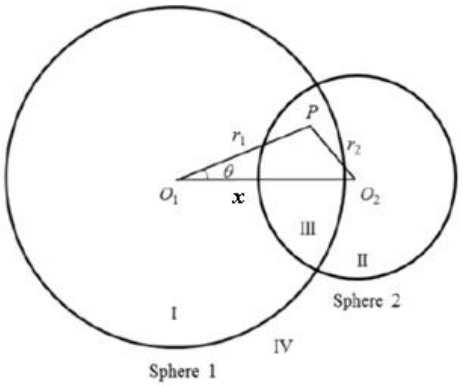

Figure B.2: Interpenetration

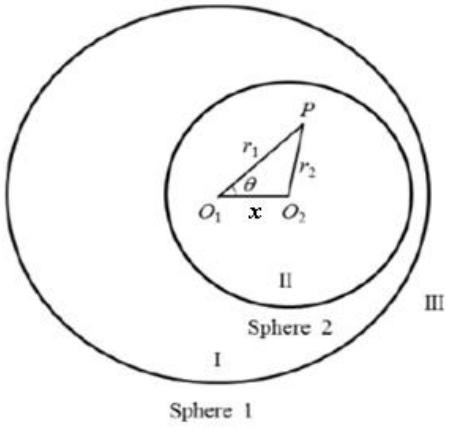

Figure B.3: Engulfing

Figure B: Three stage model for two porous spheres interacting

If dissociated groups of valence Z_j are distributed at a uniform density N_j are distributed in sphere j (j = 1, 2), then the fixed-charge density ρ_j in sphere j is related to the density N_j by $\rho_j = Z_j e N_j$ (j =1, 2). Without loss of generality, we may treat the case in which the radius R of sphere 1 is larger than or equals to the radius a of sphere 2,

$$R \geq a \qquad \text{(B.1)}$$

Ohshima assumed that the relative permittivity in spheres 1 and 2 take the same value. Permittivity (ε_r) as that of the electrolyte solution and that the electrical

potential Ψ is low enough to allow the linearization of the Poisson-Boltzmann equations for Ψ. The linearized Poisson-Boltzmann equation in the respective regions can generally be given by:

$$\Delta\Psi = \kappa^2\Psi - \frac{\rho}{\varepsilon_r\varepsilon_o} \qquad \text{(B.2)}$$

with

$$\kappa = \left(\frac{1}{\varepsilon_r\varepsilon_o kT}\sum_{i=1}^{N} z_i^2 e^2 n_i\right)^{1/2} \qquad \text{(B.3)}$$

Where κ is the Debye-Hückel parameter (*Dähnert and Rödenbeck, 1994*), $(1/\kappa)$ is the Debye length the measure of a charge carrier's net electrostatic effect in solution, and how far those electrostatic effects persist, it depends on the bulk concentration and the valence of ions

For instance z =1 for monovalent solution, z =2 for divalent, and z =3 for trivalent.

Stage 1: Interaction before contact(See Figure B.1)

$$\rho = \begin{cases} \rho_1 & for\ region\ I \\ \rho_2 & for\ region\ II \\ 0 & for\ region\ III \end{cases} \qquad \text{(B.4)}$$

Stage 2: Interpenetration (See Figure B.2)

$$\rho = \begin{cases} \rho_1 & for\ region\ I \\ \rho_2 & for\ region\ II \\ \rho_1 + \rho_2 & for\ region\ III \\ 0 & for\ region\ IV \end{cases} \qquad \text{(B.5)}$$

Stage 3: Engulfing of sphere 2 by sphere 1(See Figure B.3)

$$\rho = \begin{cases} \rho_1 & for\ region\ I \\ \rho_1 + \rho_2 & for\ region\ II \\ 0 & for\ region\ III \end{cases} \qquad \text{(B.6)}$$

The boundary conditions are:

- ✓ $\Psi \rightarrow 0$ at points far from spheres 1 and 2
- ✓ $\Psi\ and\ (d\Psi/dn)$ are continuous at the surfaces of spheres 1 and 2

The derivative of Ψ is being taken along the outward normal to the surface of each sphere. The solution to Eq. (B.2) can be expressed as the sum

$$\Psi = \Psi_1 + \Psi_2 \qquad \text{(B.7)}$$

where Ψ_1 and Ψ_2 are the unperturbed potentials for spheres 1 and 2, respectively in the absence of the interaction between the two spheres.

This is because of:

(i) Eq. (B.2) is linear with respect to Ψ and (ii) when the boundary conditions at the sphere surface are given by Eq. (B.6); the unperturbed potential of one sphere automatically satisfies the boundary conditions at the surface of the other sphere. The potential distribution Ψ for the system of two interacting ion-penetrable spheres are thus simply given by linear superposition of the unperturbed potentials Ψ_1 and Ψ_2 produced by the respective spheres. Thus one needs to solve only the potential distribution for a single isolated sphere. Consider the unperturbed potential Ψ_1 produced by sphere 1, for which Eq. (B.2) reduces to

$$\frac{d^2\Psi_{1out}}{dr_1^2} + \frac{2}{r_1}\frac{d\Psi_{1out}}{dr_1} = \kappa^2\Psi_{1out} \qquad for\ r_1 > R \qquad \text{(Outside sphere 1)} \qquad \text{(B.8)}$$

$$\frac{d^2\Psi_{1in}}{dr_1^2} + \frac{2}{r_1}\frac{d\Psi_{1in}}{dr_1} = \kappa^2\Psi_{1in} - \frac{\rho_1}{\varepsilon_r\varepsilon_o} \qquad for\ 0 \le r_1 < a_1 \quad \text{(Inside sphere 1)} \qquad \text{(B.9)}$$

$$\Psi_{1out}(r_1) \to 0 \quad as\ r_1 \to \infty \qquad \text{(B.10)}$$

$$\Psi_{1in}(R^-) = \Psi_{1out}(R^+) \qquad \text{(B.11)}$$

$$\left.\frac{d\Psi_{1in}}{dr_1}\right|_{r_1=R^-} = \left.\frac{d\Psi_{1out}}{dr_1}\right|_{r_1=R^+} \qquad \text{(B.12)}$$

where r_1 is the distance measured from the center O_1 of sphere 1. The solutions to Eq. (B.8) and (B.9) subject to Eq. (B.10) - Eq. (B.12) are:

$$\Psi_1(r_1) = \begin{cases} \Psi_{1out}(r_1)\ for\ \ r_1 \ge R \quad (ouside\ sphere\ 1) \\ \Psi_{1in}(r_1)\ for\ 0 \le r_1 \le R \ \ (inside\ sphere\ 1) \end{cases} \qquad \text{(B.13)}$$

where

$$\Psi_{1out}(r_1) = \frac{\rho_1}{\varepsilon_r\varepsilon_o\kappa^2}\left\{\cosh(\kappa R) - \frac{\sinh(\kappa R)}{\kappa R}\right\} R\,\frac{e^{-\kappa r_1}}{r_1} \qquad \text{(B.14)}$$

$$\Psi_{1in}(r_1) = \frac{\rho_1}{\varepsilon_r \varepsilon_o \kappa^2}\left\{1 - \left[1 + \frac{1}{\kappa R}\right] R e^{-\kappa R} \frac{\sinh(\kappa r_1)}{\kappa r_1}\right\} \quad \text{(B.15)}$$

Similarly, Ohshima derived the potential Ψ_2 produced by sphere 2 in the absence of sphere 1, which Ψ_2 is obtained by replacing r_1 with r_2 and R with a in Eq. (B.14) - (B.16). The result is

$$\Psi_2(r_2) = \begin{cases} \Psi_{2out}(r_2)\ for\ \ r_2 \geq a \quad (ouside\ sphere\ 2) \\ \Psi_{2in}(r_2)\ for\ 0 \leq r_2 \leq a\ \ (inside\ sphere\ 2) \end{cases} \quad \text{(B.16)}$$

where

$$\Psi_{2out}(r_2) = \frac{\rho_2}{\varepsilon_r \varepsilon_o \kappa^2}\left\{\cosh(\kappa a) - \frac{\sinh(\kappa a)}{\kappa a_2}\right\} a \frac{e^{-\kappa r_2}}{r_2} \quad \text{(B.17)}$$

$$\Psi_{2in}(r_2) = \frac{\rho_2}{\varepsilon_r \varepsilon_o \kappa^2}\left\{1 - \left[1 + \frac{1}{\kappa a}\right] a e^{-\kappa a} \frac{\sinh(\kappa r_2)}{\kappa r_2}\right\} \quad \text{(B.18)}$$

where r_2 is the radial coordinate measured from the center O_2 of sphere 2, which is related to r_1

$$r_2 = (x^2 + r_1^2 - 2x r_1 \cos\theta)^{1/2} \quad \text{(B.19)}$$

The prefactors of Eq. (B.14), (B.15), (B.17), and (B.18) are equal to the Donnan Potentials Ψ_{DON1} and Ψ_{DON2} in spheres 1 and 2, respectively. (*Dähnert and Rödenbeck, 1994*; *Ohshima*, 2010)

$$\Psi_{DONi} = \frac{\rho_i}{\varepsilon_r \varepsilon_o \kappa^2} (i = 1,2) \quad \text{(B.20)}$$

Calculations

Stage 1: Interaction between two charged porous spheres before contact

Consider two spheres 1 and 2 of radii R and a at separation x before there contact with each other, i.e. $x \geq R + a$. In this stage there are three regions I (inside sphere 1 and outside sphere 2), II (outside sphere 1 and inside sphere 2), and III (outside both spheres 1and 2) (See Figure B.1). Note that the fixed charge densities in the respective regions are ρ_1 for region I, ρ_2 for region II, and zero for region III, Eq. (B.4). The potentials in the respective regions are given by

$$\Psi = \begin{cases} \Psi_{1in}(r_1) + \Psi_{2out}(r_2)\ for\ region\ I \\ \Psi_{1out}(r_1) + \Psi_{2in}(r_2)\ for\ region\ II \\ \Psi_{1out}(r_1) + \Psi_{2out}(r_2)\ for\ region\ III \end{cases} \quad \text{(B.21)}$$

The interaction energy E_e (x) between two charged porous spheres 1 and 2 at separation x can be obtained from the free energy $F(x)$ of the system of two spheres 1 and 2 minus that at infinite separation ($x = \infty$), viz., E_e (x) = $F(x)$ - F (∞). Here $F(x)$ in stage 1 is given by

$$F(x) = \frac{1}{2}\rho_1 \int_{V_I} \Psi dV_I + \frac{1}{2}\rho_2 \int_{V_{II}} \Psi dV_{II} \qquad \text{(B.22)}$$

where integration is carried out over the volumes V_{I} and V_{II} of the respective regions I and II, and F (∞) is given by

$$F(\infty) = \frac{1}{2}\rho_1 \int_{V_I} \Psi_{1in} dV_I + \frac{1}{2}\rho_2 \int_{V_{II}} \Psi_{2in} dV_{II} \qquad \text{(B.23)}$$

This is the sum of the electrostatic self-free energies of spheres 1 and 2. We thus obtain

$$E_e(x) = F(x) - F(\infty) = \frac{1}{2}\rho_1 \int_{V_I} \Psi_{2out} dV_I + \frac{1}{2}\rho_2 \int_{V_{II}} \Psi_{1out} dV_{II} \qquad \text{(B. 22)}$$

By substituting Eq. (B.14) and (B.17) into Eq. (B.24), Ohshima obtained after some algebra

For $x \geq R + a$

$$E_e(x) = \frac{4\pi R a \rho_1 \rho_2}{\varepsilon_r \varepsilon_o \kappa^4} \left\{\cosh(\kappa R) - \frac{\sinh(\kappa R)}{\kappa R}\right\} \left\{\cosh(\kappa a) - \frac{\sinh(\kappa a)}{\kappa a}\right\} \frac{e^{-\kappa x}}{x} \qquad \text{(B.25)}$$

The interaction force $F_e(x) = -dE_e(x)/dx$ is then given by

$$F_e(x) = \frac{4\pi R a \rho_1 \rho_2}{\varepsilon_r \varepsilon_o \kappa^4} \left\{\cosh(\kappa R) - \frac{\sinh(\kappa R)}{\kappa R}\right\} \left\{\cosh(\kappa a) - \frac{\sinh(\kappa a)}{\kappa a}\right\} \frac{(\kappa x + 1) e^{-\kappa x}}{x^2} \qquad \text{(B.26)}$$

Stage 2: Interaction between two charged partially interpenetrating porous spheres

Consider two partially interpenetrating spheres 1 and 2 of radii R and a at Separation x, where $R - a < x < R + a$. In this stage there are three regions I (inside sphere 1 and outside sphere 2), II (outside sphere 1 and inside sphere 2), III (inside both spheres 1and 2), and IV (outside both spheres 1 and 2) (See Figure B.2). Note

that the fixed charge densities in the respective regions are ρ_1 for region I, ρ_2 for region II, and $\rho_1 + \rho_2$ for region III, and zero for region IV.

The potentials in the respective regions are given by:

$$\Psi = \begin{cases} \Psi_{1in}(r_1) + \Psi_{2out}(r_2)\ for\ region\ I \\ \Psi_{1out}(r_1) + \Psi_{2in}(r_2)\ for\ region\ II \\ \Psi_{1in}(r_1) + \Psi_{2in}(r_2)\ for\ region\ III \\ \Psi_{1out}(r_1) + \Psi_{2out}(r_2)\ for\ region\ IV \end{cases} \quad \text{(B.27)}$$

The free energy *F(x)* of the system of two spheres 1 and 2 in stage 2 is given by

$$F(R) = \frac{1}{2}\rho_1 \int_{V_I} \Psi dV_I + \frac{1}{2}\rho_2 \int_{V_{II}} \Psi dV_{II} + \frac{1}{2}(\rho_1 + \rho_2) \int_{V_{III}} \Psi dV_{III} \quad \text{(B.28)}$$

Thus the interaction energy $E_e(x)$ between two charged porous spheres 1 and 2 at separation x in stage 2 is

$$E_e(x) = F(x) - F(\infty) \quad \text{(B.29)}$$

$$= \frac{1}{2}\rho_1 \int_{V_I} \Psi_{2out} dV_I + \frac{1}{2}\rho_2 \int_{V_{II}} \Psi_{1out} dV_{II} + \frac{1}{2}\rho_1 \int_{V_{III}} \Psi_{2in} dV_{III} + \frac{1}{2}\rho_2 \int_{V_{III}} \Psi_{1in} dV_{III} \quad \text{(B.30)}$$

By substituting Eq. (B.14), (B.15), (B.17) and (B.18) into Eq. (B.30), Ohshima obtained after some algebra

For $R - a \le x \le R + a$

$$E_e(x) = \frac{4\pi Ra\rho_1\rho_2}{\varepsilon_r\varepsilon_o\kappa^4 x}\left[\frac{1}{\kappa^2 Ra}\left\{1 + \frac{\kappa^2}{2}(x^2 - R^2 - a^2)\right\} + \frac{\kappa^2}{24Ra}(x - R - a)^2\{x^2 + 2(R + a)x - 3(R - a)^2\} + \left[1 - \frac{1}{\kappa^2 Ra}\right]e^{-\kappa x}\cosh\big(\kappa(R - a)\big) - \left[\frac{1}{\kappa R} - \frac{1}{\kappa a}\right]e^{-\kappa x}\sinh\big(\kappa(R - a)\big) - \left[1 + \frac{1}{\kappa R}\right]\left[1 + \frac{1}{\kappa a}\right]e^{-\kappa(R+a)}\sinh(\kappa x)\right] \quad \text{(B.31)}$$

The interaction force $F_e(x) = -d\,E_e(x)/dx$ is then given by

$$F_e(x) = \frac{4\pi Ra\rho_1\rho_2}{\varepsilon_r\varepsilon_o\kappa^4 x^2}\left[\left[1 + \frac{1}{\kappa R}\right]\left[1 + \frac{1}{\kappa a}\right]\{(\kappa x + 1)e^{-\kappa(x+R+a)} + (\kappa x - 1)e^{-\kappa(x-R-a)}\} + \left[1 + \frac{1}{\kappa R}\right]\left[1 - \frac{1}{\kappa a}\right](\kappa x + 1)e^{-\kappa(x+R-a)} + \left[1 - \frac{1}{\kappa R}\right]\left[1 + \frac{1}{\kappa a}\right](\kappa x + 1)e^{-\kappa(x-R+a)} + \kappa^2 Ra\left[1 - \frac{1}{(\kappa R)^2}\right]\left[1 - \frac{1}{(\kappa a)^2}\right] - \frac{1}{\kappa^2 Ra}\{(\kappa x)^2 - 1\} - \frac{\kappa^2}{4Ra}(x^2 - R^2 - a^2)^2\right] \quad \text{(B.32)}$$

Stage 3: Interaction for the case where sphere 2 is engulfed by sphere 1

Consider two spheres 1 and 2 of radii *R* and *a* at separation *x*, where $0 \leq x \leq R- a$. So that sphere 2 is engulfed by sphere 1. In this stage there are three regions I (inside sphere 1 and outside sphere 2), II (inside spheres 1 and 2), and III (outside spheres 1 and 2). (See Figure B.3). The fixed charge densities in the respective regions are ρ_1 for region I, $\rho_1 + \rho_2$ for region II, and zero for region III. The potentials in the respective regions are given by

$$\Psi = \begin{cases} \Psi_{1in}(r_1) + \Psi_{2out}(r_2) \; for \; region \; I \\ \Psi_{1in}(r_1) + \Psi_{2in}(r_2) \; for \; region \; II \\ \Psi_{1out}(r_1) + \Psi_{2out}(r_2) \; for \; region \; III \end{cases} \tag{B.33}$$

The free energy *F(x)* of the system of two spheres 1 and 2 in stage 3 is given by

$$F(x) = \frac{1}{2}\rho_1 \int_{V_I} \Psi dV_I + \frac{1}{2}(\rho_1 + \rho_2) \int_{V_{II}} \Psi dV_{II} \tag{B.34}$$

Thus the interaction energy $E_e(x)$ between two charged porous spheres 1 and 2 at Separation *x* in stage 3 is

$$E_e(x) = F(x) - F(\infty) \tag{B.35}$$

$$E_e(x) = \frac{1}{2}\rho_1 \int_{V_I} \Psi_{2out} dV_I + \; + \frac{1}{2}\rho_1 \int_{V_{II}} \Psi_{2in} dV_{II} \; + \frac{1}{2}\rho_2 \int_{V_{II}} \Psi_{1in} dV_{II} \tag{B.36}$$

By substituting Eq. (B.15), (B.17) and (B.18) into Eq. (B.33), Ohshima obtained after some algebra

For $0 \leq x \leq R - a$

$$E_e(x) = \frac{4\pi R a \rho_1 \rho_2}{\varepsilon_r \varepsilon_o \kappa^4 x}\left[\frac{(\kappa a)^2 x}{3R} - \left[1 + \frac{1}{\kappa R}\right] e^{-\kappa R}\left\{\cosh(\kappa a) - \frac{\sinh(\kappa a)}{\kappa a}\right\}\sinh(\kappa x)\right] \tag{B.37}$$

The interaction force $F_e(x) = -dE_e(x)/dx$ is then given by

$$F_e(x) = \frac{4\pi R a \rho_1 \rho_2}{\varepsilon_r \varepsilon_o \kappa^4 x^2}\left[\{(\kappa x)\cosh(\kappa x) - \sinh(\kappa x)\}\left[1 + \frac{1}{\kappa R}\right] e^{-\kappa R}\left\{\cosh(\kappa a) - \frac{\sinh(\kappa a)}{\kappa a}\right\}\right] \tag{B.38}$$

References

- Ainalema, M. L., and Nylander, M. 2011. DNA Condensation Using Cationic Dendrimers Morphology and Supramolecular Structure of Formed Aggregates, Soft Matter, 7, pp. 4577–4594.
- Ayush, V., and Francesco, S. 2009. Effect of Surface Properties on Nanoparticle Cell Interactions, Small Volume, 6(1), pp. 12-21.
- Benoit, J., and Saxena, A. 2007. Spherical Vesicles Distorted by a Grafted Latex Bead: An Exact Solution, Phys. Rev. E: Stat., Nonlinear Soft Matter Phys. 76, pp. 364-368.
- Bernardi, G. 2004. Biochemistry of Lipids, Lipoproteins, and Membranes. 4th ed. Amsterdam, Bernardi, G., pp. 20-25.
- Bloomfield, V. A. 1996. DNA Condensation by Multivalent Cations, Curr. Opin. Struct. Biol., 6, pp. 334–341.
- Chen, H., Meisburger, S. P., Pabit, S. A., Sutton, J. L., Webb, W. W., and Pollack, L. 2012. Ionic Strength Dependent Persistence Lengths of Single Stranded RNA and DNA, Proc. Nat. Acad. Sci. USA, (109), pp. 799-804.
- Chithrani, D., Ghazani, A.A., and Vhan, W.C.W. 2006. Determining the Size and Shape Dependence of Gold Nanoparticle Uptake into Mammalian Cells, Nano Lett. 6, pp. 662-668.
- Dähnert, K., Rödenbeck, M. 1994. Exact Solution of Bisphere Debye-Huckel Problem, Journal of Colloid and Interface Science, 163, pp. 229-233.
- Dasgupta, S., Auth, T., and Gompper, G. 2013. Wrapping Ellipsoidal Nano particles by Fluid Membranes, 9, pp. 5473-5482.
- Deserno, M., and Gelbart, W. 2002. Adhesion and Wrapping in Colloid-Vesicle Complexes, J. Phys. Chem. B. 06, pp. 5543–5552.

- Dietrich, C., Angelova, M., and Pouligny, B. 1997. Adhesion of Latex Spheres to Giant Phospholipid Vesicles: Statics and Dynamics, J. Phys. II, 7, pp. 1651–1682.
- Ding, H .M., Tian, W. D., and Ma, Y. Q. 2012. Controlling Cellular Uptake of Nanoparticles with pH-Sensitive Polymers, ACS Nano, 6, pp. 1230-1238.
- Duncan, R., and Izzo, L. 2005. Dendrimer Biocompatibility and Toxicity, Adv. Drug Delivery Rev., 57, pp. 2215-2237.
- Evans, E. 1990. Adhesion of Surfactant-Membrane Covered Droplets: Special Features and Curvature Elasticity Effects, Colloids Surfaces, 43, pp. 327-347.
- Gurr, M. I., Harwood, J. L., Frayn, K. N. 2002. Lipid Biochemistry an Introduction. 5th ed. London, Blackwell Science, pp. 232-234.
- Hong, S., Bielinska, A. U., Mecke, A., Keszler, B., Beals, J. L., Shi, X., Balogh, L., Orr, B. G., Baker Jr, , J. R., and Holl, M. M. B. 2004. Positively Charged Dendron Micelles Display Negligible Cellular Interactions, Bioconjugate Chem. 15, pp. 774-782.
- Jones, S., Zhang, X. 2008. Core Signaling Pathways in Human Pancreatic Cancers Revealed by Global Genomic Analyses, Parsons Science, 321, pp. 1801-1806.
- Jonsson, M., and Linse, P. 2001. Analytical Model Study of Dendrimer-DNA Complexes, 115, pp. 10957- 10967.
- Kornberg, R. D. 1997. Structure of Chromatin, Annu. Rev. Biochem. 46, pp. 931–954.
- Kubo, K., Freitas-Ast´ ua, J., Machado, M., and Kitajima, E. 2009. Orchid Fleck Symptoms may be Caused Naturally by Two Different Viruses Transmitted by Brevipalpus, J. Gen. Plant Pathol., 75, pp. 250–255.

- Lasic, D. D. and Tcmpleton, N.S. 1997. Drug Targeting Organ-Specific Strategies in Liposomes in Gene Delivery, CRC Press, Boca Raton FL. pp. 151-165.
- Lee, H., and Larson, R. G. 2011. Effects of Salt on The Size and Internal Structure of PAMAM Dendrimers at Different pH, Macromolecules, 44, pp. 2291-2298.
- Liu, X. X., Rocchi, P., and Peng, L. 2012. Self-Association and Complexation of the Anti-Cancer Drug Doxorubicin with PEGylated Hyper-branched Polyesters in an Aqueous Environment, New J. Chem. 36, pp. 256 -263.
- Liu, Y., Tan, J., Thomas, A., Ou-Yang, D., and Muzykantov, V. 2012. Computational Modeling of Magnetic Nanoparticle Targeting to tent Surface under High Gradient Field, Therapeutic delivery, 3, pp. 181–194.
- Lodish, H., Berk, A., Zipursky, S. L., Matsudaira, P., Baltimore, D., Darnell, J. 2000. Molecular Cell Biology, 4th ed. New York: W. H. Freeman & Company. pp. 182-184.
- Luo, D., Haverstick, K., Belcheva, N., Han, E., Saltzman, W. M. 2002. Poly Ethyl Conjugated PAMAM Dendrimer for Biocompatible High efficiency Delivery, Macromolecules, 35(9), pp. 3456-3462.
- Lyulin, S. V., Darinskii, A. A., and Lyulin, A. V. 2005. Shear Induced Effects in Hyperbranched Linear Polyelectrolyte Complexes, Macromolecules, 38, pp. 3990 - 3998.
- Lyulin, S. V., Vattulainen, L., and Gurtovenko, A. A. 2008. Modeling the Formation of Ordered Nano-assemblies Comprised by Dendrimers and Linear Polyelectrolytes: The Role of Coulombic Interactions, Macromolecules. 41, pp. 4961- 4968.
- Mahato, R. I., and Kim, S.I. 2002. Pharmaceutical Perspective of Nucleic Acid-Based Therapeutics, 6th ed., London & New York: Taylor & Francis, pp.1-481.

- Maiti, P. K., and Bagchi, B. 2006. Structure and Dynamics of DNA-Dendrimer Complexation: Role of Counterions, Water, and Base Pair Sequence, Nano Lett., 6, 2478-2485.
- Marrink, S. J., Risselada, H. J. H. J., Yefimov, S., Tieleman, D. P., and de Vries, A. H. 2007. Computational Studies of Biomembrane Systems: Theoretical Considerations, Simulation Models, and Applications , J. Phys. Chem. B. 111, pp. 7812-7824.
- Ohshima, H. 2010. Biophysical Chemistry of Bio interfaces. New Jersy: John Wiley & Sons, pp.:3-6; 83-94; 133-142.
- Ohshima, H. 2013. Current Opinion in Colloid & Interfaces Sciences, 18, pp. 73-82.
- Örberg, M. L., Schillen, K., and Nylander, T. 2007. Dynamic Light Scattering and Fluorescence Study of the Interaction between Double-Stranded DNA and Poly (amidoamine) Dendrimers, Bio macromolecules, 8, 1557–1563.
- Patri, K., Kukowska-Latallo, J. F., and Baker, J. R. 2005. An Introduction to Polymeric Nanomedicines in Cancer Drug Delivery, Adv. Drug Delivery Rev. 57, pp. 2203-2214.
- Qamhieh, K., Khaleel, A. A. 2013. Analytical Model Study of Complexation of Dendrimer as an Ion Penetrable Sphere with DNA, Colloids and Surfaces, 442, pp. 191-198.
- Schiessel, H., Bruinsma, R. F., and Gelbart, W. M. 2001. Electrostatic Complexation of Spheres and Chains under Elastic Stress, J. Chem. Phys., 115, pp. 7245-7252.
- Tian, W. D., and Ma, Y. Q. 2013. Theoretical and computational studies of dendrimers as delivery vectors, Chem. Soc. Rev. 42(2), pp**.** 705–727.

- Tkachenko, A. G., Xie, H., Coleman, D., Glomm, W., Ryan, J., Anderson, M. F., Franzen, S., Feldheim, D. L. 2003. Controlled Size Manipulation of Free Gold Nanoparticles by Laser Irradiation and their Facile Bioconjugation, J. Am. Chem. Soc., 125, pp. 4700 - 4701.
- Tomalia, D. A. 2010. Dendrons/dendrimers: Quantized, Nano Element like Building Blocks for Soft-Soft and Soft-Hard Nano Compound Synthesis, Soft Matter, 6, pp. 456-474.
- Watson, J. D., and Crick, F. H. C. 1953. Molecular Structure of Nucleic Acid- a Structure for Deoxyribose Nucleic Acid, Nature, 171, pp. 737–738.
- Welch, P., and Muthukumar, M. 1998. Molecular Dynamics Study of Charged Dendrimers in Salt-Free Solution: Effect of Counterions, Macromolecules, 31, pp. 5892-5897.
- Welch, P., and Muthukumar, M. 2000. Dendrimer Polyelectrolyte Complexation: A Model Guest−Host System, Macromolecules, 33(16), pp. 6159-6167.
- Xu, L., Kuang, H., Wang, L., and Xu, C. 2011. Molecular Thinking for Nanoplasmonic Design, J. Mater. Chem., 21, pp. 16759-16782.

الملخـــــــــــــص

لقد تمت دراسة القوه المؤثره على اختراق الجسيمات الكروية لجسيمات كروية اخرى قابلة للاختراق(مسامية) مثل الاغشية المخاطية حيث يمكن لهذه الجسيمات بأن تكون ايونات صغيرة الحجم أو بروتينات أو جزيئات مصنعة . حيث نتوقع من هذه الدراسة بأن يكون لها مجال تطبيقي في علاج الجينات عن طريق الادوية ومعالجة السرطانات.
لقد تم تطوير نموذج بالاعتماد على النموذج الذي انتجه الباحثون دايترش وانجيلانوفا وبوليفي في دراستهم لاختراق جسيمات كروية لبعضها البعض باعتبار هذه الجسيمات متعادلة- لا تحمل شحنه. حيث قمنا باضافة التفاعل الكهروستاتيكي الذي طوره الباحث اكشيما الناجم من الشحنة التي تمتلكها الايونات و البروتينات وكذلك الجزيئات ولقد تبين ان التفاعل الكهروستاتيكي يؤثر بشكل كبير على زيادة الاختراق . حيث وجد ان زيادة كثافة الشحنه الحجمية يزيد من الاختراق. اما في حالة خفض تراكيز المحلول الملحي فأنه يؤدي الى زيادة الاختراق. بالنسبة لاختيار ثابت العزل فقد وجد انه كلما كان ثابت العزل منخفض كلما كانت المادة اكثر اختراقا.